AGU PUBLICATIONS

JGR

Journal of Geophysical Research: Atmospheres

RESEARCH ARTICLE
10.1002/2013JD021079

Key Point:
- Analysis of the sources and meteorological controls of PM in the WMB.

Supporting Information:
- Readme
- Tables S1 to S6

Correspondence to:
M. Pandolfi,
marco.pandolfi@idaea.csic.es

Citation:
Pandolfi, M., et al. (2014), Effects of sources and meteorology on particulate matter in the Western Mediterranean Basin: An overview of the DAURE campaign, *J. Geophys. Res. Atmos.*, *119*, 4978–5010, doi:10.1002/2013JD021079.

Received 22 OCT 2013
Accepted 3 APR 2014
Accepted article online 8 APR 2014
Published online 29 APR 2014

Effects of sources and meteorology on particulate matter in the Western Mediterranean Basin: An overview of the DAURE campaign

M. Pandolfi[1], X. Querol[1], A. Alastuey[1], J. L. Jimenez[2,3], O. Jorba[4], D. Day[2,3], A. Ortega[3,5], M. J. Cubison[2,3,6], A. Comerón[7], M. Sicard[7,8], C. Mohr[9,10], A. S. H. Prévôt[9], M. C. Minguillón[1], J. Pey[1], J. M. Baldasano[4,11], J. F. Burkhart[12], R. Seco[13,14], J. Peñuelas[13,15], B. L. van Drooge[1], B. Artiñano[16], C. Di Marco[17], E. Nemitz[17], S. Schallhart[18,19], A. Metzger[20], A. Hansel[18], J. Lorente[21], S. Ng[22], J. Jayne[23], and S. Szidat[24,25]

[1]Institute of Environmental Assessment and Water Research, Barcelona, Spain, [2]Department of Chemistry and Biochemistry, University of Colorado Boulder, Boulder, Colorado, USA, [3]Cooperative Institute for Research in Environmental Sciences, Boulder, Colorado, USA, [4]Earth Sciences Department, Barcelona Supercomputing Center–Centro Nacional de Supercomputacion, Barcelona, Spain, [5]Department of Atmospheric and Oceanic Sciences, University of Colorado Boulder, Boulder, Colorado, USA, [6]Now at Tofwerk AG, Thun, Switzerland, [7]Remote Sensing Laboratory, Signal Theory and Communications Department, Technical University of Catalonia, Barcelona, Spain, [8]Institute for Space Studies of Catalonia - Aerospace and Research Center, Technical University of Catalonia, Barcelona, Spain, [9]Laboratory of Atmospheric Chemistry, Paul Scherrer Institute, Villigen, Switzerland, [10]Now at Department of Atmospheric Sciences, University of Washington, Seattle, Washington, USA, [11]Environmental Modeling Laboratory, Technical University of Catalonia, Barcelona, Spain, [12]NILU – Norwegian Institute for Air Research, Kjeller, Norway, [13]CSIC, Global Ecology Unit CREAF-CEAB-UAB, Cerdanyola del Vallès, Spain, [14]Now at Atmospheric Chemistry Division, National Center for Atmospheric Research, Boulder, Colorado, USA, [15]CREAF, Cerdanyola del Vallès, Spain, [16]Research Centre on Energy, Environment and Technology CIEMAT, Madrid, Spain, [17]Centre for Ecology & Hydrology (Edinburgh), Penicuik, UK, [18]Institut für Ionenphysik und Angewandte Physik, Universität Innsbruck, Innsbruck, Austria, [19]Now at Department of Physical Sciences, Division of Atmospheric Sciences, University of Helsinki, Helsinki, Finland, [20]Ionicon Analytik, Innsbruck, Austria, [21]Atmospheric Physics Group of the University of Barcelona, Barcelona, Spain, [22]School of Chemical and Biomolecular Engineering and School of Earth and Atmospheric Sciences, Georgia Institute of Technology, Atlanta, Georgia, USA, [23]Aerodyne Research, Inc., Billerica, Massachusetts, USA, [24]Department of Chemistry and Biochemistry, University of Bern, Bern, Switzerland, [25]Oeschger Centre for Climate Change Research, University of Bern, Bern, Switzerland

Abstract DAURE (Determination of the Sources of Atmospheric Aerosols in Urban and Rural Environments in the Western Mediterranean) was a multidisciplinary international field campaign aimed at investigating the sources and meteorological controls of particulate matter in the Western Mediterranean Basin (WMB). Measurements were simultaneously performed at an urban-coastal (Barcelona, BCN) and a rural-elevated (Montseny, MSY) site pair in NE Spain during winter and summer. State-of-the-art methods such as ^{14}C analysis, proton-transfer reaction mass spectrometry, and high-resolution aerosol mass spectrometry were applied for the first time in the WMB as part of DAURE. WMB regional pollution episodes were associated with high concentrations of inorganic and organic species formed during the transport to inland areas and built up at regional scales. Winter pollutants accumulation depended on the degree of regional stagnation of an air mass under anticyclonic conditions and the planetary boundary layer height. In summer, regional recirculation and biogenic secondary organic aerosols (SOA) formation mainly determined the regional pollutant concentrations. The contribution from fossil sources to organic carbon (OC) and elemental carbon (EC) and hydrocarbon-like organic aerosol concentrations were higher at BCN compared with MSY due to traffic emissions. The relative contribution of nonfossil OC was higher at MSY especially in summer due to biogenic emissions. The fossil OC/EC ratio at MSY was twice the corresponding ratio at BCN indicating that a substantial fraction of fossil OC was due to fossil SOA. In winter, BCN cooking emissions were identified as an important source of modern carbon in primary organic aerosol.

1. Introduction

The Western Mediterranean Basin (WMB) is a very complex area where atmospheric dynamics, coupled to local orography and the variety of anthropogenic and biogenic sources, give rise to high pollution levels. Buildup of pollutants is favored by weak synoptic forcing characterized by anticyclonic conditions with calm winds, scarce precipitation, and prolonged exposure to intense solar radiation [see, e.g., *Lelieveld et al.*, 2002;

Ichoku et al., 2002]. Atmospheric particulate matter (PM) and precursor gases in the WMB originate from numerous areas along the coast where several large cities, industrial areas, and ports are located. Furthermore, the WMB is affected by the transport of dust from North Africa which is most frequent during summer, contributing seasonally to higher coarse particulate matter (PM) loading in the region [*Escudero et al*., 2005; *Rodríguez et al*., 2001; *Querol et al*., 1998, 2009]. A number of studies have been published on atmospheric pollution in the WMB at both coastal/urban and rural scales [e.g., *Querol et al*., 2004; *Viana et al*., 2005; *Pérez et al*., 2008a; *Pey et al*., 2010]. These studies show that during typical winter anticyclonic episodes (WAE) and summer regional recirculation scenarios, the WMB experiences severe pollution episodes affecting not only coastal areas closest to the emission sources but also rural and remote inland areas. Under WAE hourly fine PM (PM_1; particulate matter with aerodynamic diameter $< 1\ \mu m$) concentrations at regional background (RB) sites in the WMB may be occasionally higher than those simultaneously recorded at nearby urban agglomerations [*Pérez et al*., 2008a; *Pey et al*., 2009, 2010]. On a daily basis around 10% of the days under WAE typically register similar PM_1 concentrations at regional and urban/coastal scales. Considering the PM composition, high concentrations of nitrate species have been observed during these WAE episodes [*Pey et al*., 2010]. In summer the pollution episodes lead to the accumulation of pollutants on a regional scale due to the regional recirculation of air masses, whereas dilution and dispersion of PM is observed at the more local urban/coastal scale [*Pey et al*., 2009; *Pérez et al*., 2004; *Querol et al*., 2004].

DAURE (Determination of the Sources of Atmospheric Aerosols in Urban and Rural Environments in the Western Mediterranean) was a multidisciplinary international field campaign aimed at investigating the sources and meteorological controls of PM in the Western Mediterranean Basin (WMB), with particular attention to the carbonaceous fraction. Measurements were simultaneously performed at an urban-coastal (Barcelona, BCN) and a rural-elevated (Montseny, MSY) site pair in NE Spain during winter (February to March 2009; DAURE-W) and summer (July 2009; DAURE-S). Main foci of the campaign were the study of the origin of the pollution episodes and the emissions, formation, transport, and transformation of aerosols during these pollution scenarios. Particular attention was devoted to quantitatively understand the sources and formation mechanisms of secondary inorganic and organic aerosols (SIA and SOA) in the WMB and the effects of anthropogenic activities on SOA formation at local and regional levels.

Several state-of-the-art methods such as ^{14}C analysis [*Szidat et al*., 2007; *Szidat*, 2009], proton-transfer reaction mass spectrometry (PTRMS) [*Lindinger et al*., 1998] for volatile organic compounds (VOCs) and high-resolution time-of-flight aerosol mass spectrometry (HR-AMS) for fine-particle composition [*DeCarlo et al*., 2006; *Ng et al*., 2011] were applied for the first time in the Western Mediterranean region as part of DAURE, together with more traditional filter and impactor-based methods. While these state-of-the-art techniques have been applied for source apportionment studies in Northern and Central Europe [see, for example, *Jimenez et al*., 2009; *Zhang et al*., 2007; *Lanz et al*., 2010], it is unclear whether the results from these regions are applicable to the WMB due to differences in emission sources, vegetation types, and meteorological conditions. Consequently, the DAURE field campaign represents a unique opportunity for a better understanding of the behavior of regional PM concentrations and chemistry in southwestern Europe.

In this paper we present an overview of the objectives, groups involved, measurements performed, and key findings during the DAURE campaign which provides a framework for more detailed papers. In section 2 we describe the study design, typical meteorological conditions in the WMB, measurements performed, and modeling during the DAURE campaign together with a review of published results from the DAURE campaign. Section 3 is dedicated to the analysis of the different meteorological scenarios detected during DAURE-W and DAURE-S and of diurnal cycles of PM and chemical and gaseous compounds. Summary and conclusions are reported in section 4.

2. The DAURE Campaign

2.1. Study Design

Measurements were simultaneously conducted at two sites in NE Spain during winter (*DAURE-W*: 23 February to 27 March 2009, coincident with an EMEP (European Monitoring and Evaluation Programme)/EUCAARI (European Integrated project on Aerosol Cloud Climate and Air Quality Interactions) Europe-wide campaign) and summer (*DAURE-S*: 01–31 July 2009). The selected measurement sites were Barcelona (BCN), an urban, coastal site (41°23′24.01″N 02° 6′58.06″E, 80 m above sea level (asl)) and Montseny (MSY), a rural site (41°46′45.63″N 02°21′28.92″E, 720 m asl) (see Figure 1).

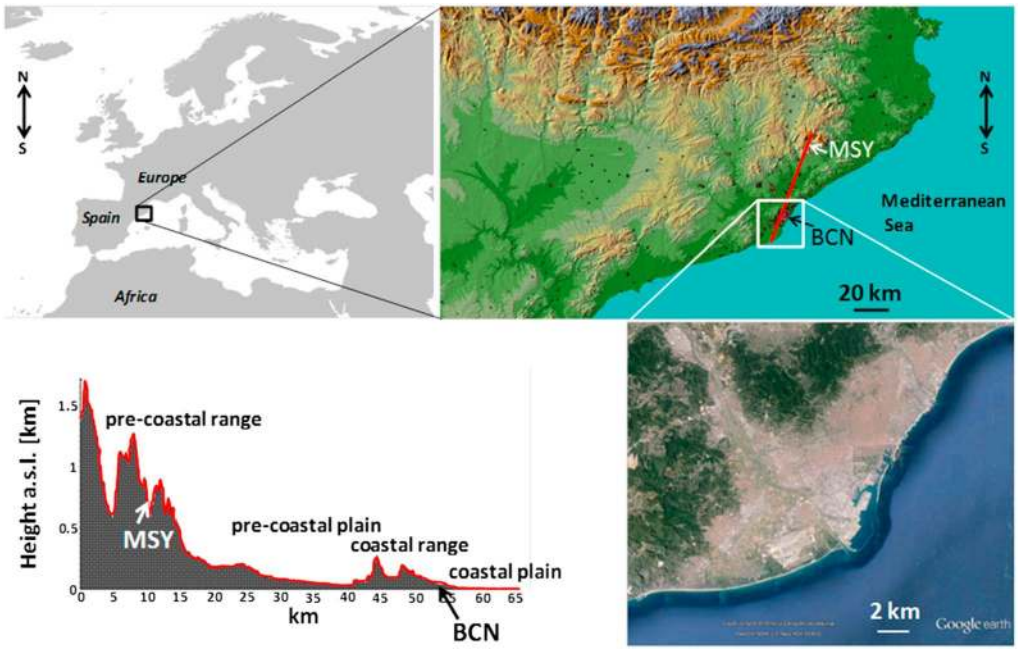

Figure 1. Location and altitude of Barcelona (BCN) and Montseny (MSY) measurement sites. Transection is also shown and highlighted with the red color.

The area selected for the DAURE campaign is a highly populated region with around 4.5 million inhabitants mostly concentrated in the Barcelona metropolitan area. Barcelona (101 km^2 with 1.6 million inhabitants) has one of the highest car densities in Europe with more than 6000 vehicles per square kilometer (http://www.dgt.es/portal/es/seguridad_vial/estadistica/parque_vehiculos/por_provincia_tipo_y_carburante). Moreover, several industrial areas and power plants are present and numerous busy highways cross the area making it one of the most polluted areas in the WMB [*Pey et al.*, 2009]. According to the annual report of the Autonomous Government of Catalonia, in 2009 in the Barcelona Metropolitan Area exceedances of the European annual limit values were observed for NO_2 (annual limit value 40 $\mu g/m^3$; exceedances observed at 40% of the stations) and PM10 (annual and daily limit values (DLV) 40 $\mu g/m^3$ and 50 $\mu g/m^3$ more than 35 days per year, respectively; exceedances at 25% and 40% of the stations, respectively). Ozone exceedances of the threshold for the protection of human health (180 $\mu g/m^3$ on hourly basis) were detected during a total of 60 h distributed in 25% of the stations in the whole Catalonia region. Currently, the PM10 DLV is exceeded in a smaller number of stations compared with 2009, whereas NO_2 concentrations are still exceeded in around 30% of the stations. The implementation of European Union (EU) abatement strategies and national/local measures for pollutant emission reduction led to a progressive reduction of PM concentrations at EU level [*Cusack et al.*, 2012; *Barmpadimos et al.*, 2012]. Despite this, the EURO4 and EURO5 standards were less effective for the abatement of NO_x concentrations [*Querol et al.*, 2013].

In Barcelona, traffic and residential (heating and cooking) emissions and activities such as construction and demolition, in addition to industrial emissions, dictate the degree of air pollution although not with the same contributions. Studies in Barcelona show traffic accounting for up to 50% of the average annual levels of PM [*Amato et al.*, 2009a], whereas about 70% of NO_x emissions are produced by combustion from vehicles.

In Barcelona the measurements were conducted in the western part of the city, about 0.5 km away from the Diagonal Avenue, one of the main roads of the city. This site is representative of urban background conditions, influenced by vehicular emissions.

The Montseny site is part of the EUSAAR (European Supersites for Atmospheric Aerosol Research) network (www.eusaar.net), succeeded in March 2011 by the ACTRIS network (Aerosols, Clouds, and Trace gases Research InfraStructure Network), and was created to standardize and integrate the measurements of atmospheric aerosol properties at European ground-based stations. MSY is a RB monitoring site located within a regional natural park about 50 km to the NNE of the city of Barcelona and 25 km NW of the Mediterranean coast.

Journal of Geophysical Research: Atmospheres
10.1002/2013JD021079

Table 1. Participant Groups During DAURE-W and DAURE-S Campaigns

Participant Groups	Country	Site	Campaigns	Technique	Parameter	Notes
CSIC	Spain	BCN	DAURE-W	Optical counter	1 h PM_{10}, $PM_{2.5}$, and PM_1	PM concentrations corrected
(National Research Council)	BCN	MSY	DAURE-S	(Grimm)		with gravimetric measurements
				High-volume	12 h to 24 h speciation	Inductively Coupled Plasma Mass
				samplers	of PM_{10}, $PM_{2.5}$, and PM_1	Spectrometry (ICP-MS), Inductively Coupled Plasma Atomic Emission Spectroscopy (ICP-AES) for concentrations of sulfate, nitrate, chloride, ammonium, Ca, Al, Fe, K, Mg, Mn, P, Ti, and 55 trace elements. OC and EC by a SUNSET Analyser. Organic tracer compounds by conventional solvent extraction-GC-MS technique.
				MAAP[a]	Black carbon mass concentration	
				CPC[b]	particles number (#/cm^3)	Size range: 10–800 nm
				Meteo data	Wind speed and direction, T, RH, precipitation, solar radiation	Data from a meteorological tower at 10 m high
CEH (Centre for Ecology and Hydrology)	Scotland, UK	MSY	DAURE-W DAURE-S	Annular Rotating Batch Denuder	NH_3, NO_3, HNO_3, HONO, HCl, H_2O_2	1 h resolution
CEH / University of Colorado	Scotland (UK)/ Colorado (CU)	MSY	DAURE-W	HR-ToF-AMS[c]	Organics, NO_3^-, $SO_4^=$, NH_4^+, Cl^-	Submicron aerosol mass loading measurements
PSI (Paul Sherrer Institute)	Switzerland	BCN	DAURE-W	HR-ToF-AMS[c]	Organics, NO_3^-, $SO_4^=$, NH_4^+, Cl^-	Submicron aerosol mass loading measurements
				Aethalometer	Black carbon mass concentration @ 880 nm	PSI in charge for the ^{14}C analysis from PM1 filters collected from CSIC
				SMPS[e]	Aerosol size concentration and distribution	Aerosol size range: 9–615 nm; 116 bins
		MSY	DAURE-W	Rotating Drum Impactor	PM_1, $PM_{1-2.5}$, $PM_{2.5-10}$	Hourly resolved elemental aerosol composition
		Mobile Lab	DAURE-W	HR-ToF-AMS, MAAP, CPC, CO_2, FMPS[j]	Organics, NO_3^-, $SO_4^=$, NH_4^+, Cl^- Black carbon concentration; particles number (#/cm^3); particle size distribution	On route particle measurements
BSC (Barcelona Supecomputing Center)	Spain	BCN MSY	DAURE-W DAURE-S	WRF/CMAQ/DREAM Computer Program	Air quality, mineral dust, meteorological modeling	
CREAF (Centre for Ecological Research and Forestry Applications)	Spain	BCN (MSY)	DAURE-W DAURE-S (DAURE-S)	PTR-Quad-MS[f]	Real-time VOC measurements	
Ion Chemistry Group, University of Innsbruck,	Austria	MSY	DAURE-W	PTR-ToF-MS[g]	Real-time VOC measurements	
CIEMAT (Centre for Energy, Environment and Technology Research)	SPAIN	BCN	DAURE-W DAURE-S	Particulate nitrate[h] and sulfate[i] analyzer	Real-time sulfate and nitrate concentrations	
			DAURE-W	Cascade impactor MOUDI	Two samples day/night per day NO_3^-, SO_4^{2-}, NH_4^+, Cl^-	IC analysis of samples at 10 stages from 10–18 mm to 0.056–0.1 mm.
				Low volume sampler with $PM_{2.5}$ cutoff.	Individual particles size & morphological parameters	SEM/EDS analysis
		MSY	DAURE-W	SMPS	Aerosol size concentration and distribution	Aerosol size range: 17–594 nm; 100 bins

Table 1. (continued)

Participant Groups	Country	Site	Campaigns	Technique	Parameter	Notes
UPC (Universitat Politècnica de Catalunya)	SPAIN	BCN	DAURE-W DAURE-S	Lidar[d]	Aerosol backscatter and extinction coefficient vertical profiles	@ 532 nm and 1064 nm
UB (University of Barcelona)	SPAIN	BCN	DAURE-W DAURE-S	Cimel sunphotometer and Radiosounding	Aerosol optical depth and vertical P, T, RH, wind mes.	Sunphotometer wavel. @ 440, 670, 870, 936,1020 nm
Aerodyne Research, Inc	Boston, USA	MSY	DAURE-W	ACSM[k]	Organics, NO_3^-, $SO_4^=$, NH_4^+, Cl^-	Submicron aerosol mass loading measurements
			DAURE-W	Meteo data	Wind speed and direction, T, RH, pressure	

[a]Multiangle absorption photometer.
[b]Condensation particle counter.
[c]High-resolution time-of-flight aerosol mass spectrometry.
[d]Light detection and ranging.
[e]Scanning mobility particle sizer.
[f]High sensitivity proton transfer reaction quadrupole mass spectrometer.
[g]Proton-transfer reaction time-of-flight mass spectrometer.
[h]Model R&P8400N.
[i]Model Thermo 5020i SPA.
[j]Fast mobility particle sizer spectrometer.
[k]Aerosol chemical speciation monitor.

A detailed description of the measurement sites and previous measurements of aerosol concentration and composition can be found in the literature for the MSY [e.g., *Pérez et al*., 2008a; *Pey et al*., 2009] and BCN stations [e.g., *Pey et al*., 2008; *Pérez et al*., 2008b].

Main topographical features of the area under study include the following: (1) the coastal plan which contains most of the cities in the Barcelona metropolitan area in the 8 km strip of land between the sea and the first mountain range, (2) the coastal mountain range with peaks around 500–650 m, (3) the precoastal plan between the mountain coastal ranges, and (4) the precoastal mountain range where the MSY station is located (Figure 1).

2.2. Meteorology

The complex layout of the coast in the WMB and the frequently weak synoptic forcing favors the development of mesoscale, thermally driven flows which originate from the upslope winds driven by the sea breeze in the morning and which return back to the sea in the evening. This pattern has the potential to form stratified residual layers of aged pollutants which subside over the coastal area and the sea [e.g., *Millán et al*., 1997; *Gangoiti et al*., 2001; *Pérez et al*., 2004]. In summer, due to the intense and rapid solar heating of the lower atmospheric layers, the convergence of surface winds from the coast to the central plateau injects polluted air into the middle troposphere up to 3.5–5 km [*Millán et al*., 1991; *Pérez et al*., 2004]. The summer meteorology is highly influenced by the Azores high-pressure system located over the Atlantic Ocean that induces very weak synoptic pressure gradients over the WMB which allow the regional recirculation and accumulation of aerosol in the absence of Atlantic advection. Moreover, African dust intrusions are more frequent during summer [*Rodríguez et al*., 2001; *Querol et al*., 1998; *Pey et al*., 2013].

Accumulation of PM over the WMB in winter takes place when the Azores high moves toward the WMB, residing over this area for several days. This results in weak synoptic winds, and stagnation of polluted air masses persists over the WMB allowing emissions to accumulate and age over the region. Occasionally, the Azores high moves south giving rise to the flow of Atlantic low-pressure and frontal systems into the Mediterranean [*Lopez-Bustins et al*., 2008]. Advection of Atlantic air masses during the cold season clears out the previously accumulated stagnated air masses, leading to lower pollutant concentrations at regional scale.

2.3. Measurements

The participating research groups and the instruments deployed by each group during DAURE are listed in Tables 1 and 2. Several state-of-the-art real-time instruments were deployed including three HR-AMS (placed at BCN and MSY measurement sites and in a mobile laboratory for on-road measurements); one aerosol chemical speciation monitor (ACSM; deployed at MSY); two different proton transfer reaction mass spectrometers (PTRMS): a proton transfer reaction time-of-flight mass spectrometer (PTR-ToF-MS) [*Graus et al*., 2010] at MSY in winter and a high sensitivity proton transfer reaction quadrupole mass spectrometer (PTR-Quad-MS) [*Lindinger et al*., 1998; *Filella and Peñuelas*, 2006] at MSY in summer and at BCN in both summer and winter.

The HR-AMS and ACSM performs real-time measurements of nonrefractory (NR) submicron aerosol species including sulfate, nitrate, ammonium, chloride, and organic aerosol (OA) [*DeCarlo et al*., 2006]. The sum of these chemical components will be referred to as NR-PM1. The OA time series of the mass spectra from HR-AMS can be further analyzed using positive matrix factorization (PMF) to apportion the total OA to several components, representing different sources and processing. These components include oxygenated OA (OOA), a surrogate for secondary OA; hydrocarbon-like OA (HOA), a surrogate for primary chemically reduced OA (POA);

Table 2. Collaborating Groups During DAURE-W and DAURE-S Campaigns

Collaborating Groups	Country	Site	Campaigns	Tasks
GenCat (Departament de Medi Ambient, Generalitat de Catalunya)	Spain	BCN	DAURE-W	Gas phase measurements
		MSY	DAURE-S	
FMI (Finnish Meteorological Institute)	Finland	BCN	DAURE-W	Llevoglucosan analyses from filters in collaboration with CSIC
		MSY	DAURE-S	
RJL (RJ Lee Group Inc.)	US	BCN	DAURE-W	Electron microscopy in collaboration with CIEMAT
		MSY	DAURE-S	
NILU (Norvegian Institute for Air Research)	Norway	BCN	DAURE-W	FLEXPART trajectory model results[a]
		MSY	DAURE-S	
CNR-ISAC (National Research Council – Institute of Atmospheric Sciences and Climate)	Italy	BCN	DAURE-W	Analysis of the water-soluble organic carbon by NMR[b]
		MSY	DAURE-S	
University of Berne		BCN	DAURE-W	^{14}C analysis
		MSY	DAURE-S	
University of Aveiro	Portugal	BCN	DAURE-W	Analysis of molecular markers
		MSY	DAURE-S	
University of Pannonia	Hungary	BCN	DAURE-S	Analysis of molecular markers
		MSY	DAURE-S	
Agencia Nacional de Meteorologia, Instituto de Salud Carlos III, Ministerio de Medio Ambiente	Spain		DAURE-W	As part of EMEP, they will analyze samples coordinated with DAURE from stations in Huelva (Southwest Spain) and Risco Llano (Central Spain)
			DAURE-S	

[a]Through the EUCAARI (European Integrated project on Aerosol Cloud Climate and Air Quality Interactions) collaboration.
[b]Nuclear magnetic resonance.

and biomass burning OA (BBOA) [*Zhang et al*., 2005; *Jimenez et al*., 2009; *Lanz et al*., 2010]. BBOA is thought to be dominated by biomass burning (BB) POA (primary OA), while SOA (secondary OA) formed from BB emissions is apportioned to the OOA [*DeCarlo et al*., 2010; *Cubison et al*., 2011].

The PTR-Quad-MS and the PTR-ToF-MS perform measurements of volatile organic compounds (VOCs) emitted into the atmosphere from both natural and anthropogenic sources and involved in ozone (O_3) production and SOA formation. Measurements include the concentration of traffic-related compounds such as toluene (*m/z* 93), benzene (*m/z* 79), the biomass-burning tracer acetonitrile (*m/z* 42), and the biogenic compounds, monoterpenes (*m/z* 137) and isoprene (*m/z* 69). Other contributions to these *m/z* are thought to be minor [*de Gouw and Warneke*, 2007].

The fossil versus nonfossil fractions of organic carbon (OC) and elemental carbon (EC) at both field sites were investigated by analyzing isotopic carbon ratios of the particles collected on PM1 filters with high-volume samplers [*Zhang et al*., 2012; *Minguillón et al*., 2011; *Szidat et al*., 2007; *Szidat*, 2009].

These state-of-the-art methods were combined with classical PM measurements for the determination of PM_x loadings (PM_{10}, $PM_{2.5}$ and PM_1) on a 1 h basis using real-time optical counters (Grimm) [*Querol et al*., 2008a] and PM_x gravimetric measurements (12 h or 24 h) with high-volume samplers (30 m^3/h) and appropriate cutoff inlets. PM_x samples collected on quartz fiber filters were analyzed following the experimental procedures described in *Querol et al*. [2001] for the concentrations of major elements (Al, Ca, K, Mg, Fe, Ti, Mn, P, S, and Na) and 46 trace elements, as well as NO_3^-, SO_4^{2-}, NH_4^+, and Cl^- ion concentrations. Concentrations of OC and EC were determined from the filters following the EUSAAR2 protocol [*Cavalli et al*., 2010] with a Sunset OC/EC Field Analyzer (RT 3080, Sunset Laboratory Inc., USA) [*Bae et al*., 2004]. The concentrations of organic matter (OM) on filters were obtained by multiplying OC by the OM:OC ratios (method details in *Aiken et al*. [2008]) determined by elemental analysis of the HR-AMS mass spectra. OM:OC average ratios of 2.0 and 1.6 were determined for MSY and BCN, respectively [*Minguillón et al*., 2011; *Mohr et al*., 2012]. Mineral matter was calculated by summing Al_2O_3, SiO_2 (calculated as $3 \times Al_2O_3$), CO_3^{2-}, Ca, Fe, K, Mg, Mn, Ti, and P, while marine aerosol was the sum of Na and Cl. Marine sulfate contributes only little to marine aerosols in the area under study [i.e., *Querol et al*., 2008b]. The indirect determination of CO_3^{2-} concentrations was obtained using the ion balance as described in *Querol et al*. [2009] and *Karanasiou et al*. [2008]. Several PM1 filter samples were analyzed for organic tracer compounds after solvent extraction and chemical analysis by gas chromatography coupled to mass spectrometry (GC-MS) [*van Drooge et al*., 2012].

Black carbon (BC) mass concentrations and particle number concentrations were measured with multiangle absorption photometers (MAAP) and condensation particle counters (CPC), respectively, at both sites.

The aerosol optical depth and the vertical profiles of aerosol backscatter and extinction coefficients were measured at BCN with a Cimel sunphotometer, which is part of the NASA Aerosol Robotic Network [*Holben et al*., 1998], and an elastic/Raman lidar (light detection and ranging) [*Rocandebosh et al*., 2000], which is part of the European Aerosol Research LIDAR Network-Advanced Sustainable Observation System network [*Pappalardo et al*., 2007] (now ACTRIS under the EC 7th Framework Programme; www.actris.net), respectively. Both instruments were located about 600 m east of the BCN measurement site.

Real-time measurements of gaseous pollutants were acquired by conventional air pollution monitors (Thermo Scientific, Model 42i for NO_x and MCV S.A., model 48AUV for O_3).

Ground wind speed and direction, temperature, relative humidity, precipitation, and solar radiation were also measured at both sites with conventional meteorological sensors. The vertical profiles of atmospheric temperature, pressure, and relative humidity were obtained by radiosoundings performed twice per day (at 12:00 UTC and 00:00 UTC) at the radiosounding station also located 600 m SW of the BCN site. Data from radiosoundings were used for the determination of the mixing layer height (MLH at 12:00 UTC) and residual layer height (RLH at 00:00 UTC) by means of the simple parcel method [*Holzworth*, 1964].

2.4. Modeling

DAURE measurements were complemented by meteorological and air quality forecasting, in addition to postcampaign modeling. Details are given in *Jorba et al*. [2013]. Daily high-resolution meteorological and air quality forecasts for the domain of study were provided by the CALIOPE (operational air quality forecasting system for Spain) modeling system [*Baldasano et al*., 2008; *Jorba et al*., 2013], and high-resolution meteorological fields were obtained from the WRF-ARW (Weather Research and Forecasting Model) model v3.0.1.1 (meteorological driver of the CALIOPE system). The study of the transport of the sampled air masses to the measurement stations was performed with the FLEXPART Lagrangian particle dispersion model [*Stohl et al*., 2005] used in backward mode [*Stohl et al*., 2003]. The output of the FLEXPART (FLEXible PARTicle dispersion model) simulations, using input data from the European Centre for Medium-Range Weather Forecasts (ECMWF) at $1° \times 1°$ resolution, is a time- and space-resolved emission sensitivity field, which is proportional to particle residence time. Here we used the footprint emission sensitivity in the lowest model layer (0–100 m) to show where surface emission sources could have influenced the sampled air masses and the total column emission sensitivity to better show the transport not only where the air had surface contact. With the available input data from ECMWF, FLEXPART does not adequately resolve local-scale circulations such as the sea breeze and its interaction with topography. However, it informs about the larger-scale transport affecting the measurement stations. Given that FLEXPART does not resolve very well the relatively small distance between BCN and MSY stations, the simulated transport to the two stations is in most cases very similar (not shown). Consequently, both the footprint emission sensitivity and the total column emission sensitivity will be presented only for MSY station.

Saharan dust intrusions were identified by using back trajectories of air masses (HYSPLIT4 (Hybrid Single Particle Lagrangian Integrated Trajectory Model)) [*Draxler and Rolph*, 2003]; geopotential height maps (NOAA/ESRL - Earth System Research Laboratory Physical Sciences Division, Boulder, Colorado; http://www.cdc.noaa.gov/); aerosol dust concentration maps (BSC-DREAM8b - Barcelona Supercomputing Center - Dust REgional Atmospheric Model 8 bin: http://www.bsc.es/projects/earthscience/DREAM/, NAAPS - Navy Aerosol Analysis and Prediction System: http://www.nrlmry.navy.mil/aerosol/ and SKIRON - Greek weather forecasting modelling system: http://forecast.uoa.gr/dustindx.php); and satellite imagery (NASA-SeaWiFS Project: http://oceancolor.gsfc.nasa.gov/SeaWiFS/).

2.5. HR-AMS Versus PM_1 Filters

The comparison between secondary inorganic aerosols (SIA: SO_4^{2-}, NO_3^-, and NH_4^+) and OM and OC concentrations from HR-AMS and from PM1 filters, are reported in Figure 2 for DAURE-W for BCN (Figure 2a) and MSY (Figure 2b). The comparison of SIA components showed good correlation with correlation coefficients (R^2) ranging between about 0.76 and 0.90 for NO_3^- and NH_4^+ and about 0.9 for SO_4^{2-} at both BCN and MSY. The concentrations obtained with the filter analysis and HR-AMS were consistent for NH_4^+ at both sites and for SO_4^{2-} at MSY, while NO_3^- was higher for the HR-AMS at both sites, presumably due to some evaporation from the filter samples during sampling. On average, SO_4^{2-} measured by filter analysis was less than measured with HR-AMS at BCN (around 34% less). The NO_3^- HR-AMS/Filter ratios were about 1.7 at both MSY and BCN. For OM,

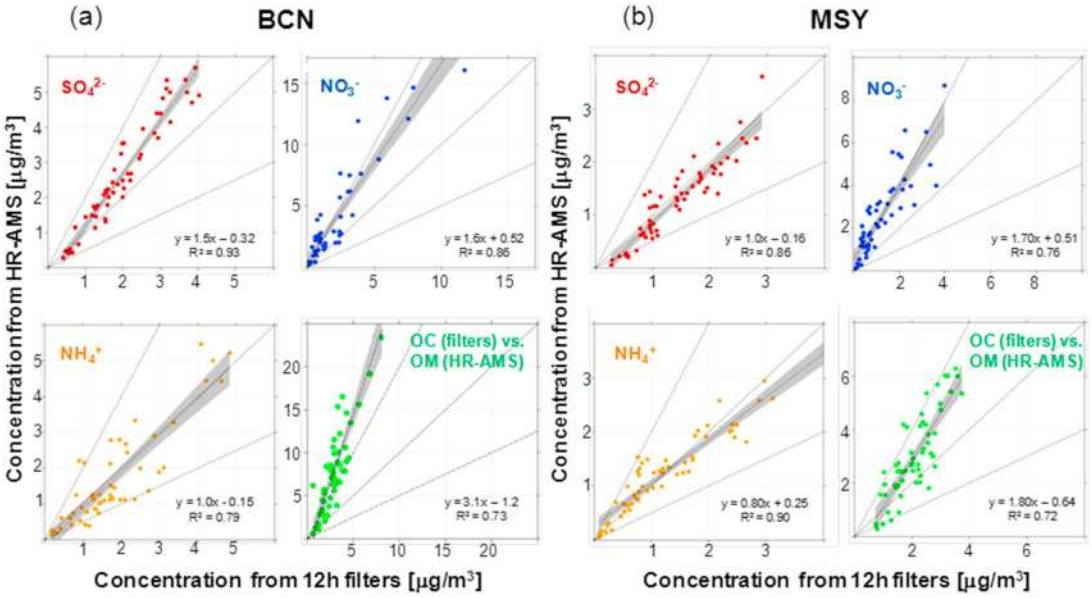

Figure 2. Comparison between SIA (SO_4^{2-}, NO_3^-, and NH_4^+) and OM versus OC concentrations in PM1 at (a) BCN and (b) MSY as measured by HR-AMS and conventional chemical procedure (12 h filters) during DAURE-W.

the slope of the regression line which can be interpreted as the organic-mass-to-organic-carbon (OM:OC) ratio was higher at BCN (~3) compared with MSY (1.8). Recent studies support values ranging between 1.6 and 2.2 for this ratio [e.g., *Zhang et al*., 2005; *Takegawa et al*., 2005; *Chen and Yu*, 2007]. The OM:OC ratio from HR-AMS/filters at MSY was close to the mean OM:OC (2.0) measured with the HR-AMS [*Minguillón et al*., 2011], while at BCN the HR-AMS/filters OM:OC ratio doubled the ratio measured by the HR-AMS (1.6 [*Mohr et al*., 2012]), For both comparisons R^2 was high (~0.7 at MSY and BCN). We do not know the reasons for the discrepancies between filters and AMS for OM:OC and SO_4^{2-} at BCN. These may have been due to higher than usual uncertainties in the HR-AMS or to possible underestimation of OC by Sunset instruments which may occur at certain threshold carbon loads as recently reported by *Zheng et al*. [2014]. However, these discrepancies do not affect the main conclusions reported in this work.

2.6. Review of Published DAURE Results

2.6.1. EC and OC Sources

Radiocarbon (^{14}C) analysis combined with PMF analysis of HR-AMS data showed that at BCN, 87% and 91% of the fine EC, during DAURE-W and DAURE-S, respectively, had fossil origin, whereas at MSY these percentages were 66% and 79%, respectively [*Minguillón et al*., 2011]. In absolute values, the difference is larger with absolute concentration of fossil EC at the urban site (1.4 μg/m^3 during DAURE-W and 1.1 μg/m^3 during DAURE-S), 6.3 and 4.5 times that at the rural site during DAURE-W and DAURE-S, respectively. The high contribution of fossil fuel combustion to EC in BCN is mainly due to road traffic which strongly influences concentration and evolution of EC (and BC) in Barcelona [*Pérez et al*., 2010; *Reche et al*., 2011a]. The higher relative contribution of nonfossil EC in winter compared to summer was attributed to higher emissions from residential wood-based heating and open burning of agricultural biomass (banned annually by law from 15 March to 15 October, Spanish Decree 64/1995). Wild fires were expected to have a low contribution (http://www.fire.uni-freiburg.de/inventory/stat/es/fire_stat_es.htm).

The relative contribution of fossil sources to OC at BCN and MSY was 40% and 31%, respectively, in winter and 48% and 25%, respectively, in summer [*Minguillón et al*., 2011]. The absolute fossil OC concentrations in winter at BCN (~1.4 μg/m^3) were slightly higher than in summer (~0.9 μg/m^3) due to stronger accumulation of pollutants under reduced dispersion, whereas at MSY the concentrations (~0.5–0.6 μg/m^3) were similar for both seasons. The higher nonfossil OC in winter at BCN (60%) than in summer (52%) was probably due to a higher contribution of biomass burning in winter, whereas at MSY the nonfossil OC was higher in summer (75%) compared to winter (69%) due to a higher contribution of biogenic emissions.

During both seasons the lower BCN/MSY ratio for fossil OC concentrations (2.1–2.4) compared with the corresponding fossil EC ratio (4.5–6.3) is consistent with formation of fossil SOA driven by photochemical reactions during transport from urban and regional sources to the MSY site. Moreover, the fossil OC/EC ratio at MSY (~2.3) for both seasons was double the corresponding ratios at BCN (~0.9) indicating that a substantial fraction of the fossil OC may be due to fossil SOA formation [*Minguillón et al*., 2011].

2.6.2. HR-AMS PMF Analysis

PMF analysis of high-resolution HR-AMS organic-mass spectra during DAURE-W identified five components of OA at BCN [*Mohr et al*., 2012] and three components at MSY [*Minguillón et al*., 2011]. At BCN these components were low-volatility oxygenated OA (28% of OA), related to regional, aged secondary OA; semivolatile oxygenated OA (27%), a fresher oxygenated OA; hydrocarbon-like OA (HOA; 16%), related mainly to traffic emissions and probably partially to ship emissions; biomass burning OA (BBOA; 11%) from domestic heating or agricultural biomass burning activities; and cooking OA (17%). At MSY the three OA components were OOA (86% of OA), HOA (4%), and BBOA (10%).

On the basis of the OM:OC ratios determined by high-resolution analysis of the AMS mass spectra, BCN fossil OC was 47% primary and 53% secondary, whereas at MSY fossil OC was estimated to be 85% secondary consistent with previous conclusions based on the higher fossil OC/EC ratio at MSY than at BCN [*Minguillón et al*., 2011]. Moreover, the OOC (oxygenated organic carbon), a surrogate for total secondary OC, was found to be mostly nonfossil at both BCN (~60%; mainly from biogenic sources, biomass burning, and urban nonfossil sources) and MSY (~70%; from biogenic sources or biomass burning). The percentage of fossil OC at both BCN and MSY was comparable to the contributions reported for central and northern Europe [*Minguillón et al*., 2011]. Thus, although it may be expected that fossil sources may have a higher influence in the WMB due to the lesser use of wood burning for residential heating, biogenic SOA from VOCs emissions driven by higher temperatures in WMB may compensate for the differences in both fossil and nonfossil OC sources. Furthermore, for Barcelona the PMF-AMS analysis revealed the potential role of cooking emissions for the organic-mass concentrations, a source which has not been fully investigated yet and may be responsible for the high fraction of modern carbon in primary organic aerosol in BCN [*Mohr et al*., 2012].

2.6.3. VOCs Measurements

At MSY, the short-chain oxygenated VOCs, and especially the biogenic isoprenoids (isoprene and monoterpenes), were around 1 order of magnitude higher in summer (averages ~0.5 and 0.7 ppbv for isoprene and monoterpenes, respectively) compared to winter (~0.04 and 0.03 ppbv, respectively) as a result of the vegetation's greater physiological activity and emission rates during the warm season [*Seco et al*., 2011, 2013]. The high concentrations of reactive VOCs and the increased photochemical activity led to higher maximum diurnal concentrations of O_3 in summer (64 ppbv) than in winter (47 ppbv) at MSY [*Seco et al*., 2011]. Some aromatic VOCs, normally linked to anthropogenic sources, such as benzene and toluene had similar mixing ratios in summer (averages ~0.07 and 0.27 ppbv for benzene and toluene, respectively) and winter (~0.14 and 0.18 ppbv, respectively). Among the measured VOC concentrations, the highest mixing ratios in both winter and summer at the rural site were observed for methanol (averages of 4.9 ppbv in summer [*Seco et al*., 2011]).

During DAURE-W VOC mixing ratios at BCN were always higher than at MSY with the exception of acetone, acetic acid, and ethanol which were detected in similar or slightly higher concentrations at MSY [*Seco et al*., 2013]. Interestingly, the mixing ratios of isoprene (average ~0.23 and 0.04 ppbv at BCN and MSY, respectively) and monoterpenes (~0.42 and 0.026 ppbv at BCN and MSY, respectively), both considered predominantly biogenic, were higher at BCN. This may be due to the fact that the emissions of isoprene and monoterpenes by the dominant tree species at MSY, holm oak, were very low in winter [*Llusia et al*., 2012], whereas emissions from anthropogenic sources were relevant in urban locations. As reported by *Seco et al*. [2013], isoprene has also known anthropogenic sources such as automobile exhaust which can be important in urban areas such as BCN. The same is true for monoterpenes [*Hellén et al*., 2012; *Seco et al*., 2013]. In summer, though, both emission rates and atmospheric mixing ratios of monoterpenes and isoprene increased by 1 order of magnitude at the rural site [*Seco et al*., 2011], while the summer monoterpene mixing ratios at BCN were in the same range as those in winter [*Seco et al*., 2013]. In BCN, the highest mixing ratios of most of the VOCs (including isoprene) in winter occurred during rush hour, indicating that traffic was the main source of most of the analyzed VOCs. Aromatic compounds, mainly toluene (average ~1.6 ppbv), benzene (0.4 ppbv), and C8 aromatics (~1.7 ppbv), have a clear traffic-related origin and were the most abundant VOCs in the urban atmosphere. Other VOCs, such as the short-chain oxygenated VOCs, have multiple atmospheric sources [*Seco*

et al., 2007], such as direct emissions by vegetation, vehicles, and secondary production by degradation of other VOCs, and showed less sharp peaks during the rush hours. Monoterpenes concentrations (~0.4 ppbv) also showed an increase during rush hours. However, the highest monoterpenes mixing ratio was observed at night. Thus, other biogenic sources for monoterpenes cannot be ruled out [*Seco et al*., 2013]. At night the lowering of the planetary boundary layer (PBL), the reduced wind speed, and the cessation of photochemical destruction favored the accumulation of monoterpenes transported during the night from the nearby (~1 km away) Collserola mountains or emitted by trees of a small urban park close to the measurement station.

At BCN, all VOCs had lower mixing ratios between the two peaks (morning and evening) related to the rush hours. Reduced VOC mixing ratios in the afternoon in Barcelona were due to the cleansing effect of the sea breeze and to the height of the PBL which rose during the day, thus helping to dilute the VOC concentrations. Conversely, at the rural site, most of the measured VOCs were advected by the midday sea breeze which transported polluted air masses from the coastal plains and the metropolitan area of Barcelona to MSY, yielding the highest daily VOC mixing ratios (e.g., acetaldehyde, isoprene, benzene, and toluene with averages up to 0.65, 0.07, 0.19, and 0.41 ppbv, respectively). At MSY, only biogenic monoterpenes showed a clear local origin with concentrations rising before the development of the sea breeze.

2.6.4. BBOA Estimation

BBOA in the Barcelona region can be emitted by regional agricultural open fires and from wood-combustion heating systems in suburban and rural areas [*Reche et al*., 2012]. Biomass burning contributions to OA during DAURE-W and DAURE-S were estimated using different techniques, including ^{14}C [*Minguillón et al*., 2011], factor analysis of AMS organic spectra [*Mohr et al*., 2012; *Minguillón et al*., 2011], levoglucosan analysis [*van Drooge et al*., 2012], and receptor modeling of offline filter PM_1 and $PM_{2.5}$ data [*Minguillón et al*., 2011; *Reche et al*., 2012]. The results from these techniques were consistent, with the different estimates highly or moderately correlated. Primary biomass burning (P-BBOA) contributions to OA from filter analyses by tracer-based method using levoglucosan (levoglucosan/OCBBsource = 0.1) ranged between 0.2 and 1.4 $\mu g/m^3$ at MSY and from 0.3 to 1.0 $\mu g/m^3$ at BCN [*van Drooge et al*., 2012] and showed a moderate correlation (slope = 1; $R^2 = 0.6$) with BBOA from AMS analysis. Correlations were also observed between the following: (i) the concentrations of *n*-alkanes from PM1 filters and the HOA source contributions from PMF-AMS analysis ($R^2 = 0.5$) and (ii) dicarboxylic acids, mostly related to SOA formation [i.e., *Heald et al*., 2010], and OOA from PMF-AMS [*van Drooge et al*., 2012].

2.6.5. Trace Metals Concentrations

As with VOCs, diurnal cycles of trace metals of anthropogenic origin (associated with traffic and industrial emissions: V, Pb, Cu, Zn, Mn, Sn, Bi, Sb, and Cd) all showed an increase during the morning at MSY to a single, prolonged afternoon peak as contaminated air transported by the sea breeze moves into the mountains [*Moreno et al*., 2011]. Mainly as a consequence of this transport, the concentrations of these inhalable technogenic trace metals at MSY had upper continental crust (UCC) normalized values (ppm metal in sample/ppm metal in UCC) higher than 1 in both PM1 and PM10 fractions and during both seasons [*Moreno et al*., 2011]. At MSY in winter the relative increase between night (21:00–09:00 UTC) and day (09:00–21:00 UTC) for these technogenic metals ranged between around 140% for traffic-related elements such as Sn (average ~ 0.8 ng/m^3 at night) and Sb (~ 0.4 ng/m^3, night) to around 20% for Zn of industrial origin (~ 36 ng/m^3, night). In summer the mean concentrations of most PM_{10} inhalable metals at MSY were higher than in winter due to the effect of a thicker PBL facilitating the intrusion of contaminated urban plumes higher into the mountains. Conversely, during winter in Barcelona the average concentrations of Pb (11 ng/m^3), Cu (26 ng/m^3), Zn (65 ng/m^3), Mn (18 ng/m^3), Bi (0.4 ng/m^3), Sb (3 ng/m^3), and Cd (0.3 ng/m^3) in PM10 were all >40% higher than in summer due to the higher dispersion in summer compared with winter.

At BCN, hourly metal concentrations were controlled either by traffic (rush hour double peak for Cu, Sb, Sn, and Ba) or industrial plumes (morning peak of Zn, Ni, Mn, and Cr generated outside the city overnight) [*Moreno et al*., 2011]. The roadside enrichment for primary traffic emission tracers such as EC, Fe, Ba, Cu, Sb, Cr, and Sn of atmospheric pollutants at BCN were higher than 70% [*Amato et al*., 2011]

2.6.6. Modeling

Results from DAURE along with those of multiple other European sites were compared to the regional model COSMO-ART (Online Coupled Regional Scale Model System to treat the Dispersion of Aerosols and Reactive Trace Gases) by *Knote et al*. [2011]. The model captured the general features of the HR-AMS concentration time series, driven by the meteorology, and tended to underpredict sulfate (due to lack of cloud processing) and overpredict nitrate (partially due to the underprediction of sulfate). At MSY the simulated total organics

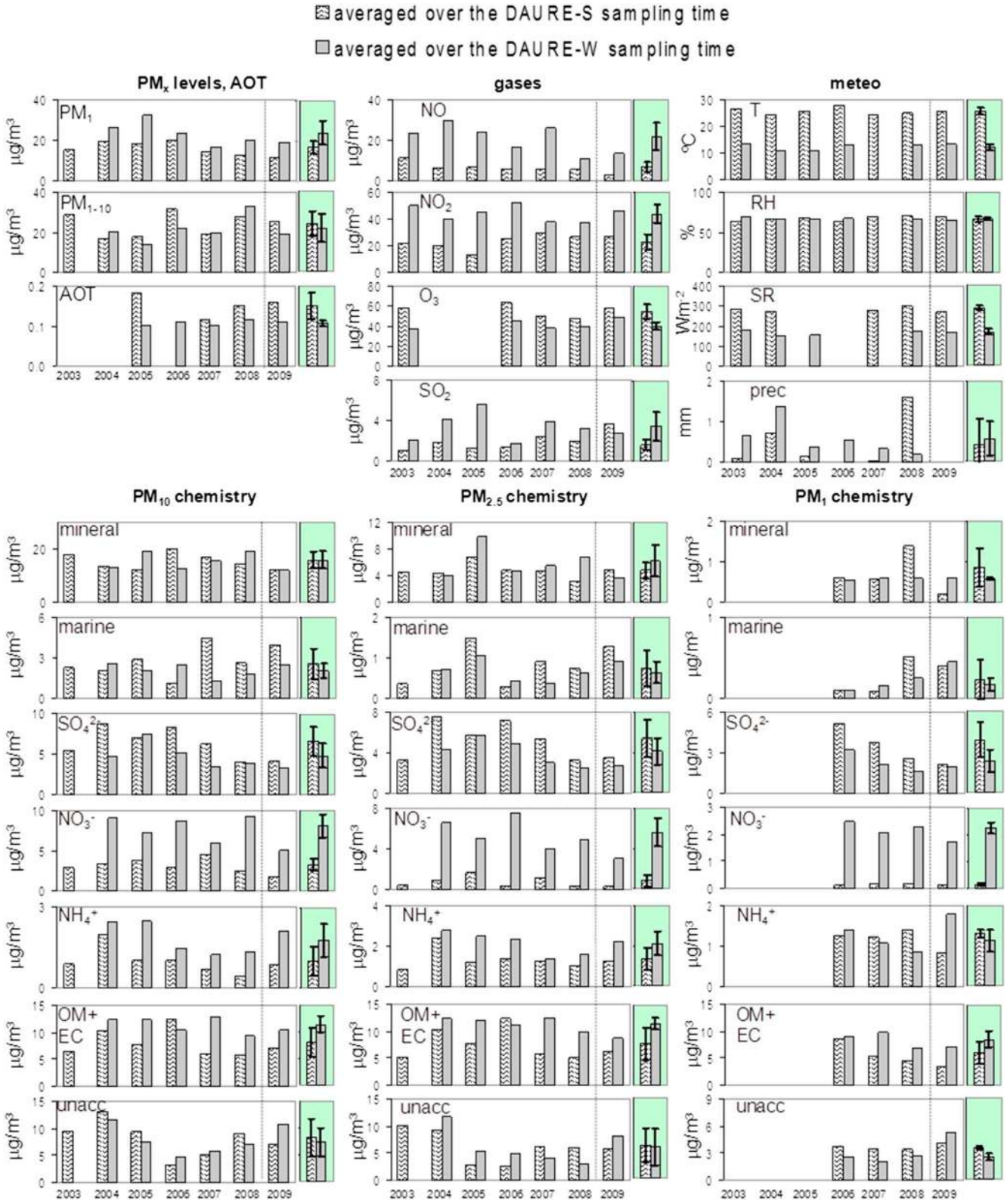

Figure 3. Representativeness of the DAURE-W and DAURE-S campaigns for Barcelona for PM_x and main chemical components concentrations; NO, NO_2, O_3, and SO_2 concentrations; aerosol optical thickness (AOT) at 675 nm; temperature; relative humidity; solar radiation; and precipitation. The 2003–2008 averages (± 1σ) are highlighted in green.

are comparable throughout the period, although the PMF analysis [*Minguillón et al.*, 2011] gives about 5% mass contribution from urban primary organics, instead of about 30% as given in the model. On average simulate nitrates were lacking the diurnal cycle visible in the measurement at MSY. As with MSY, in BCN the model produced a similar variability of HR-AMS measurements, although it overestimates nitrate, whereas sulfate levels were comparable at BCN with a large influence from shipping. OA concentrations were overestimated at BCN due to a strong overprediction of POA, while SOA were underpredicted.

3. Results

3.1. Representativeness of DAURE-W and DAURE-S

In order to assess whether the atmospheric conditions during the DAURE campaigns at both BCN and MSY were representative of the typical WMB winter and summer conditions, the levels of atmospheric components and parameters measured during DAURE-W and DAURE-S were compared with previous measurements over the years 2003–2009 (Figures 3 and 4). This comparison was carried out for the parameters with long data records available at BCN and MSY such as PM_x (PM_1 and PM_{1-10}) concentrations and chemical composition, aerosol optical thickness (AOT), gaseous pollutant concentrations, and meteorological data. In this comparison it should be taken into account that a general decreasing trend of PM_x over the last decade across Europe has been observed due to a concomitance of factors including the implementation of EU abatement strategies and national/local measures for pollutant emission reduction and meteorology [*Cusack et al.*, 2012; *Barmpadimos et al.*, 2011].

As shown in Figures 3 and 4 most of the average values calculated during the DAURE-W and DAURE-S campaigns are within one standard deviation of the 2003–2008 mean values, thus demonstrating the representativeness of the DAURE 2009 intensive measurements. Exceptions were observed for PM_{1-10} concentrations measured at MSY, which were relatively high during DAURE compared with previous years likely due to the lack of substantial precipitation during both DAURE-W and DAURE-S; and for PM_1, mineral matter, NO_3^- and NO concentrations at BCN which were slightly lower during DAURE than recent averages. These differences may be partially due to the new location selected for the BCN measurement station starting in 2009, which is less affected by direct road traffic emissions. At both BCN and MSY slightly lower SO_4^{2-} concentrations were also observed. Finally, higher unaccounted PM mass (fraction unaccounted for by chemical analysis mainly due to non-C atoms and water associated with particles) was observed for the PM_1 fraction at BCN and for the PM_{10} and $PM_{2.5}$ fractions at MSY during both DAURE-W and DAURE-S campaigns. In all these cases the unaccounted PM mass was approximately 30% of PM_x mass.

3.2. DAURE-W Campaign

3.2.1. PM_1 Scenarios

Three types of winter scenarios, named A, B, and C, during DAURE-W were identified by comparing the PM_1 concentrations measured at BCN and MSY as shown in Figure 5. Figure 5 also shows the wind speed measured at both BCN and MSY and the MLH and RLH at BCN. The estimated MLHs and RLHs were assumed to be representative of the area under study even though differences between BCN and MSY may exist given the complex orography of the area. Mean meteorological conditions, PM_1 concentrations, and MLHs and RLHs during the entire DAURE-W campaign and the A, B, and C scenarios are reported in the supporting information.

3.2.1.1. A Scenario

The A scenario was defined as periods when concentrations of PM_1 at MSY was similar (or even higher during short periods) to those at BCN. These periods included the most severe pollution episodes affecting the regional background site during DAURE-W. PM_1 concentrations ranged from 12 (BCN) and 11 $\mu g/m^3$ (MSY) during the 20–23 March period to 42 (BCN) and 41 $\mu g/m^3$ (MSY) on 28 February (Table S1). As shown later, the high variability in PM_1 concentrations observed during the A episodes at both stations were likely related to the degree of recirculation of air masses over the area under study before arriving at the measurement sites. The mean PM_1 concentration at MSY under the A scenario (18 $\mu g/m^3$) was higher than the annual mean PM_1 concentrations (11 $\mu g/m^3$) measured during the period 2002–2008 [*Pey et al.*, 2010]. A common characteristic of the A scenarios was the position of the MSY station systematically within both the diurnal MLH (839–1780 m) and the nocturnal RLH (712–920 m; Figure 5iii and Table S1). These high inversions caused the dilution of pollutants at BCN and favored the mixing of polluted air masses to the MSY altitude. Thus, both stations were on average affected by similar atmospheric dynamics and source emissions as indicated by the similarity of PM concentrations at both sites (Figure 5). The days under A scenario were typically sunny at BCN except for the

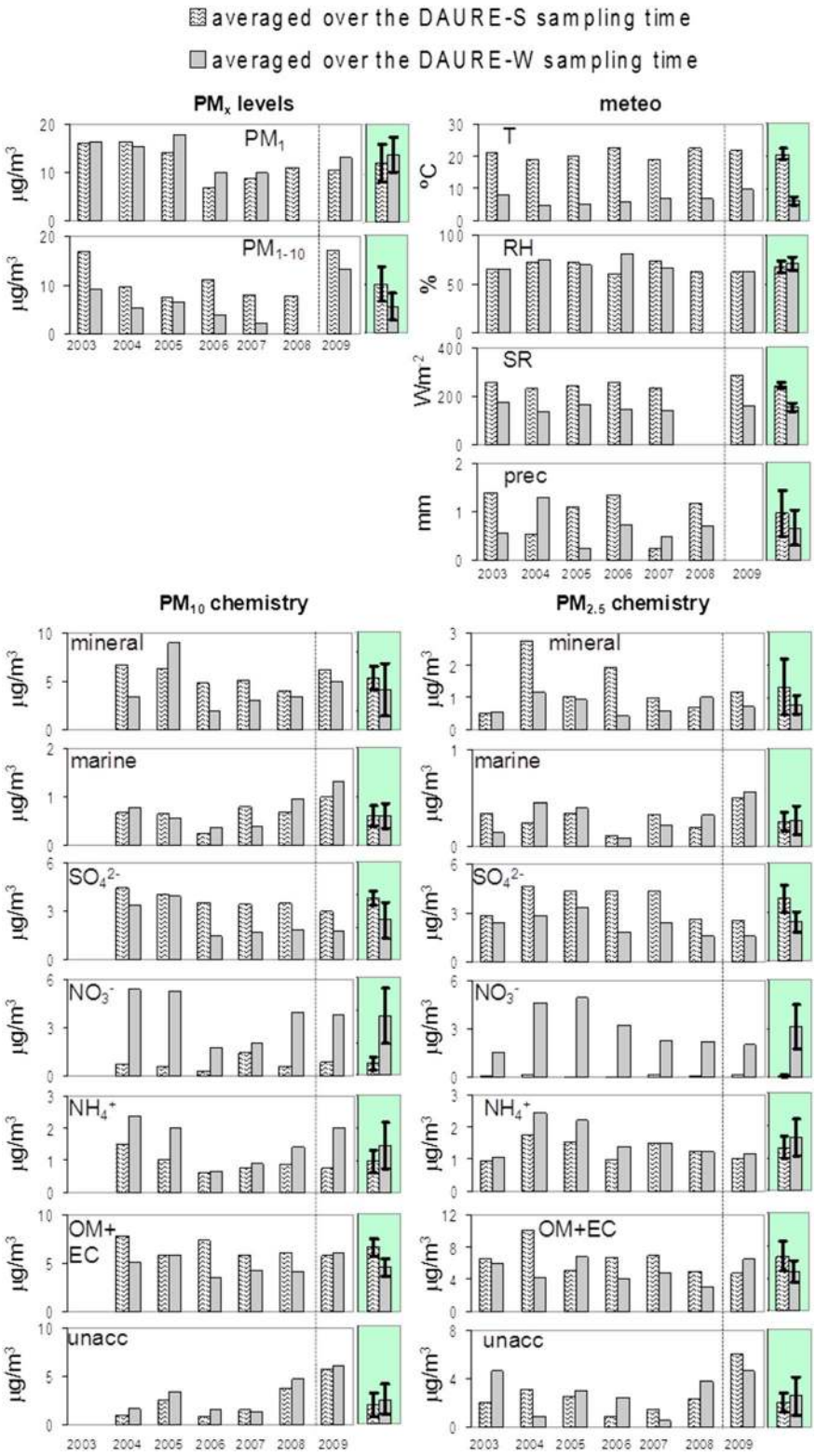

Figure 4. Representativeness of the DAURE-W and DAURE-S campaigns for Montseny for PM_x and main chemical components concentrations and meteorological data. The 2003–2008 averages (± 1σ) are reported in the colored graphs. No previous measurements of gas concentrations, AOT, and PM1 chemical composition were available before the 2009 DAURE campaigns at the MSY site.

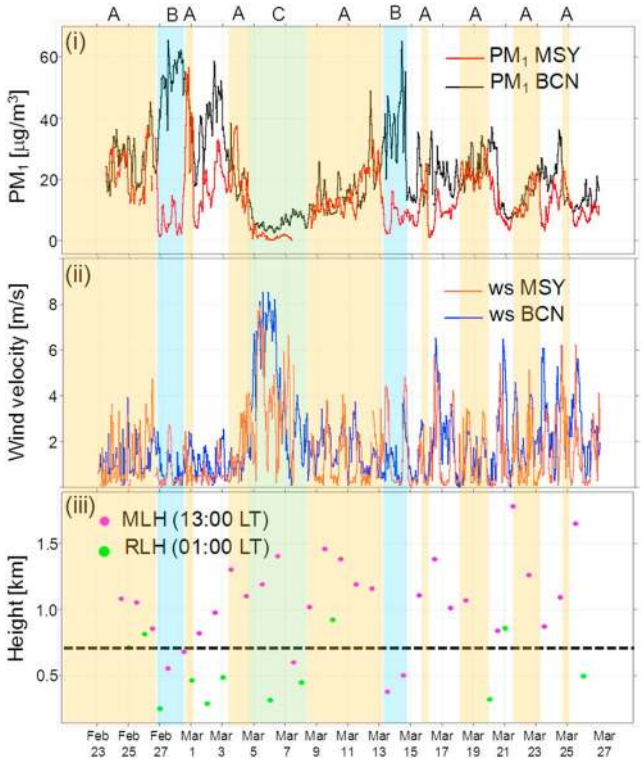

Figure 5. (i) PM1 Grimm corrected mass concentration levels at BCN and MSY, (ii) wind velocity at BCN and MSY, and (iii) PBL heights over Barcelona. Colored shadings indicate different atmospheric scenarios; MLH (mixing layer height) and RLH (residual layer height) estimated from radiosondes data at 00:00 and 12:00 GMT.

period of 03–04 March when the presence of clouds led to high relative humidity (RH) (~77%) and low solar radiation (~133 W/m^2) and wind speed (1.2 m/s). Thus, the effect of the sea breeze in transporting pollutants toward MSY was reduced under these cloudy days. Consequently, the relative effect of more local sources, the formation of aerosol species in clouds at MSY, and/or photochemical SOA production could be important as suggested by the higher PM_1 levels measured at MSY (22 μg/m^3) compared to BCN (18 μg/m^3). As shown in *van Drooge et al.* [2012], the lowest hopanes concentrations (μhopanes = 0.39 ng/m^3) were measured under these cloudy days, suggesting low influence of traffic at MSY. Conversely, high BBOA and OOA contributions were observed.

3.2.1.2. B Scenario

Conditions when the PM_1 concentrations were high at BCN and low at MSY defined the B scenario. At BCN, mean PM_1 concentrations under the two observed B scenarios were 48 μg/m^3 and 36 μg/m^3, much higher than the mean value of about 19 μg/m^3 measured at BCN for all seasons [*Pérez et al.*, 2008b], while MSY was much cleaner (6 μg/m^3 and 8 μg/m^3; cf. Figure 5i and Table S1). During the two observed B scenarios the MLHs (378–678 m) and RLHs (250 m) were the lowest observed during DAURE-W indicating the presence of a strong/medium atmospheric inversion producing the trapping of emissions in the boundary layer and thus leading to high concentrations of PM_1 at BCN. As discussed in the next section, the accumulation of pollutants was favored by strong atmospheric anticyclonic conditions, characteristic of the B scenario. At the same time, the MSY station was above the polluted PBL thus leading to a decoupling of MSY from regional PBL and thus the observed low PM1 concentrations at MSY. Also, the lowest RH values (around 33–38%) were measured at MSY during the two B scenarios (contrary to 65–68% RH measured at BCN) thus confirming that MSY was above the PBL. Both temperature and solar radiation were relatively high during the B episodes due to clear sky conditions.

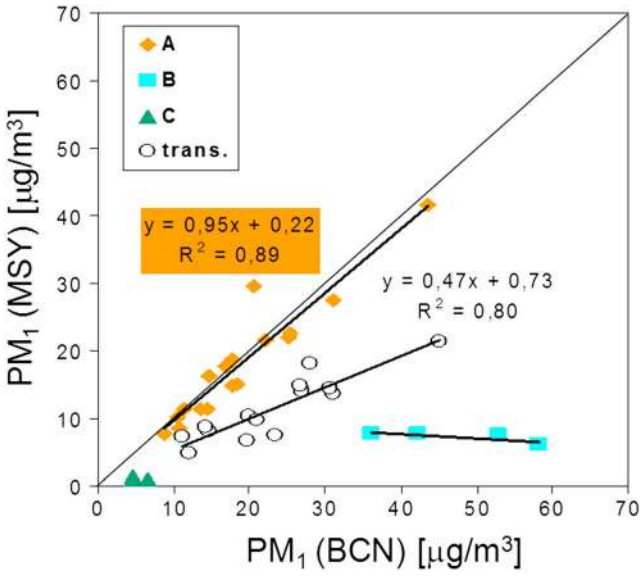

Figure 6. Cross correlation between simultaneous daily PM1 averages at Montseny (MSY) and Barcelona (BCN) during DAURE-W episodes.

3.2.1.3. C Scenario

The C scenario was defined as the period when the lowest PM_1 values were observed at both BCN (5 μg/m^3) and MSY

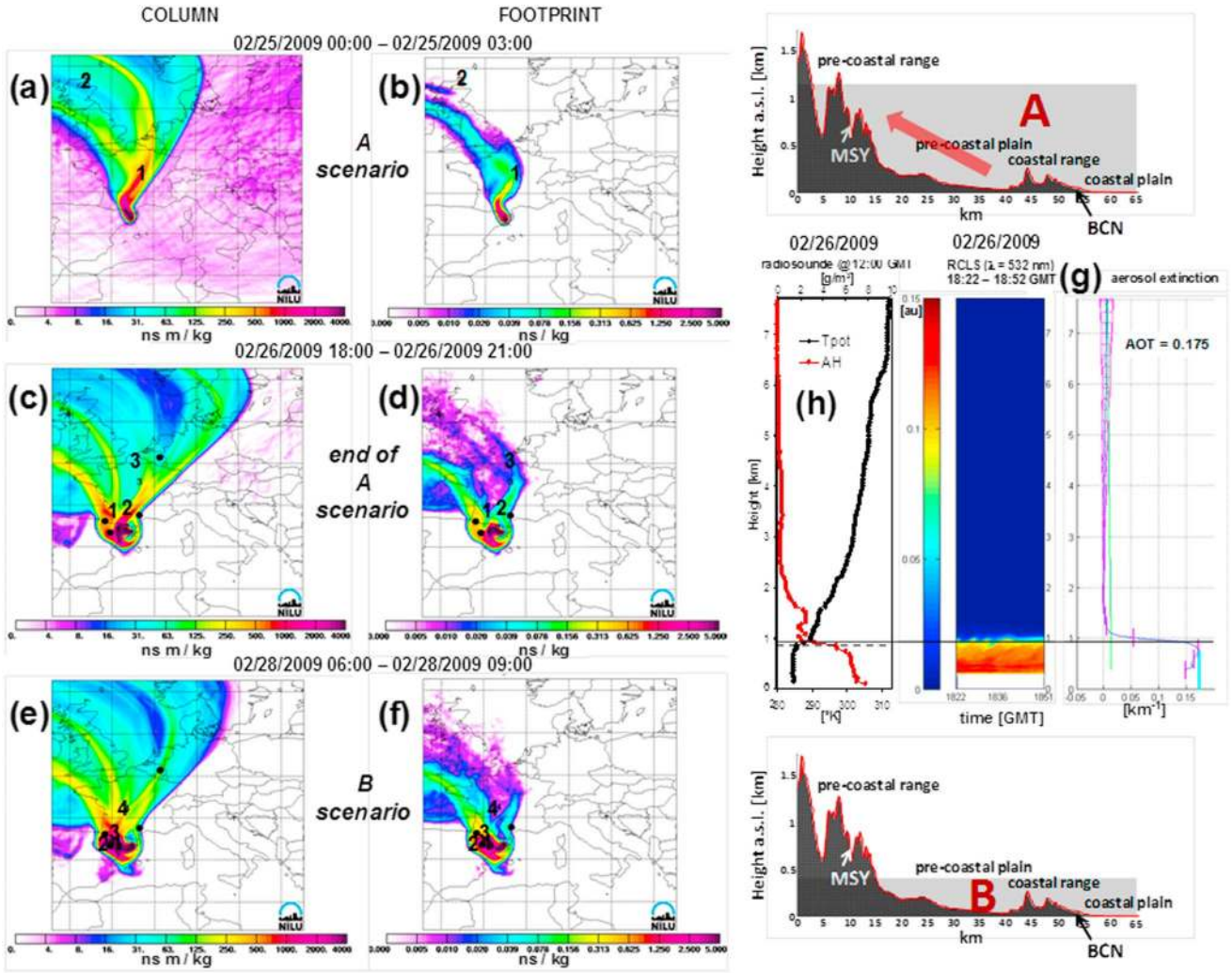

Figure 7. (a–f) FLEXPART column integrated and footprint emission sensitivities for MSY (upper/lower release height 720 m) calculated during the first A and B episodes on 25 February (00:00–03:00 GMT), 26 February (18:00–21:00 GMT), and 28 February (06:00–09:00 GMT); numbers within FLEXPART maps indicate the location of the air masses in number of days before arriving at the measurement site; (g) range-corrected lidar signal (RCLS) and aerosol extinction vertical profile from lidar measurement performed at BCN from 18:22 to 18:52 GMT on 26 February with horizontal line indicating MLH. Figures in the upper and lower right sketch the position of MSY station within (A) or above (B) the PBL; (h) vertical profiles of potential temperature (Tpot) and absolute humidity (AH) from radiosounding launched at BCN at 12:00 GMT on 26 February with horizontal dotted line indicating mixing layer height (MLH).

(1.4 μg/m^3). The C scenarios were North Atlantic Advection episodes frequently observed during the cold seasons in the WMB [e.g., *Pey et al*., 2010]. Relatively high wind speed (> 4.0 m/s) and solar radiation and relatively low temperatures and humidity characterized the C scenario. No correlation between PM1 concentrations and MLH or RLH was observed during the C scenario because of the dominant cleaning effect of the strong horizontal advection. Thus, the PBL was flushed by the advection, and low PM concentrations were measured at both measuring stations regardless of the MLH and RLH.

The A, B, and C scenarios were punctuated by transition periods (1–2 days) in which the concentrations of PM1 were always higher at the urban background and increasing at the regional background site during the afternoon when PBL was high and the sea breeze fully developed. Thus, the transition periods were characterized by relatively low RLHs (less than 500 m) and high MLHs (820–1650 m).

The comparison between the daily mean PM1 concentrations at BCN and MSY as a function of the defined scenarios (Figure 6) shows good correlation for the A scenario ($R^2 = 0.89$), with a regression slope close to 1, again supporting the coupling of the airmasses at both sites, and for the transition period ($R^2 = 0.8$) showing a concentration ratio of 1:2 (MSY:BCN). During the B episodes the regression line is almost horizontal with high

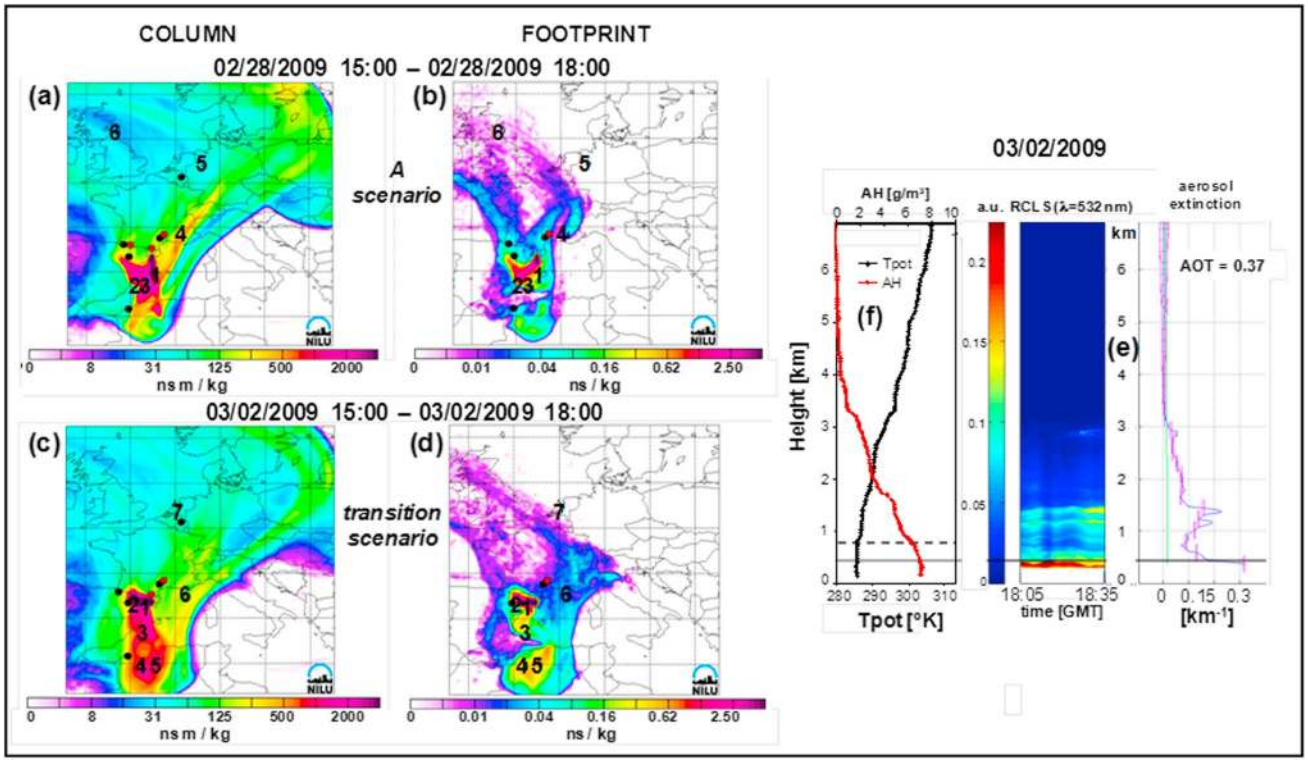

Figure 8. (a–d) FLEXPART column integrated and footprint emission sensitivities for MSY (upper/lower release height 720 m) calculated on 28 February (15:00–18:00 GMT) and 2 March (15:00–18:00 GMT); numbers within FLEXPART maps indicate the location of the air masses in number of days before arriving at the measurement site; (e) range-corrected lidar signal (RCLS) and aerosol extinction vertical profile from lidar measurement performed at BCN on 2 March (18:05–18:35 GMT) with horizontal line indicating MLH from lidar; (f) vertical profiles of potential temperature (Tpot) and absolute humidity (AH) from radiosounding launched at BCN on 2 March at 12:00 GMT with horizontal dotted line indicating MLH from radiosounding.

PM_1 concentrations at BCN always observed along with low simultaneous and rather constant PM_1 concentrations at MSY. Finally, the small group (green triangles) around the center of the axes represent the lowest PM_1 concentrations measured at both stations during the C episode.

3.2.2. A, B, and C Meteorological Scenarios

The dominant meteorological conditions affecting the WMB during the A, B, and C scenarios are summarized in this section by using the air mass back trajectories from the FLEXPART model, lidar measurements, and radiosounde data. Since the top of the boundary layer is often associated with strong gradients of aerosol content, the time evolution of the range-corrected lidar signals (RCLS) and the aerosol extinction vertical profiles are used for the determination of the PBL heights. The PBL heights from lidar are compared with the MLHs from radiosoundings.

Figure 7 presents several pieces of information about the atmospheric conditions during the first days of the campaign (23–28 February 2009) when the first A and B episodes took place. At night on 25 February air masses arrived from France and the UK (Figures 7a and 7b) and showed a tendency toward recirculation by the end of the A episode on 26 February (Figures 7c and 7d). Correspondingly, the concentrations of PM1 increased with time at both stations (Figure 5i). The lidar measurements performed on 26 February, toward the end of the first A episode, showed the presence of a high PBL around 900 m with a mean AOT of 0.175 (Figure 7g). The reported AOT is consistent with the mean AOT reported for Barcelona during February-March from 3 years (2007–2009) of lidar measurements [*Sicard et al.*, 2011]. The MLH from the radiosounding launched 6 h before the lidar measurement was only slightly lower (855 m), thus confirming a relatively constant PBL height during this period (Figure 7h). During the B episode on 28 February the air masses recirculated even more residing for about 3–4 days over the area under study (Figures 7e and 7f). The PM_1 concentrations at BCN increased, while the decrease in the PBL height was responsible for the decrease of PM_1 at MSY despite the general strong anticyclonic conditions in the WMB (cf. Figure 5).

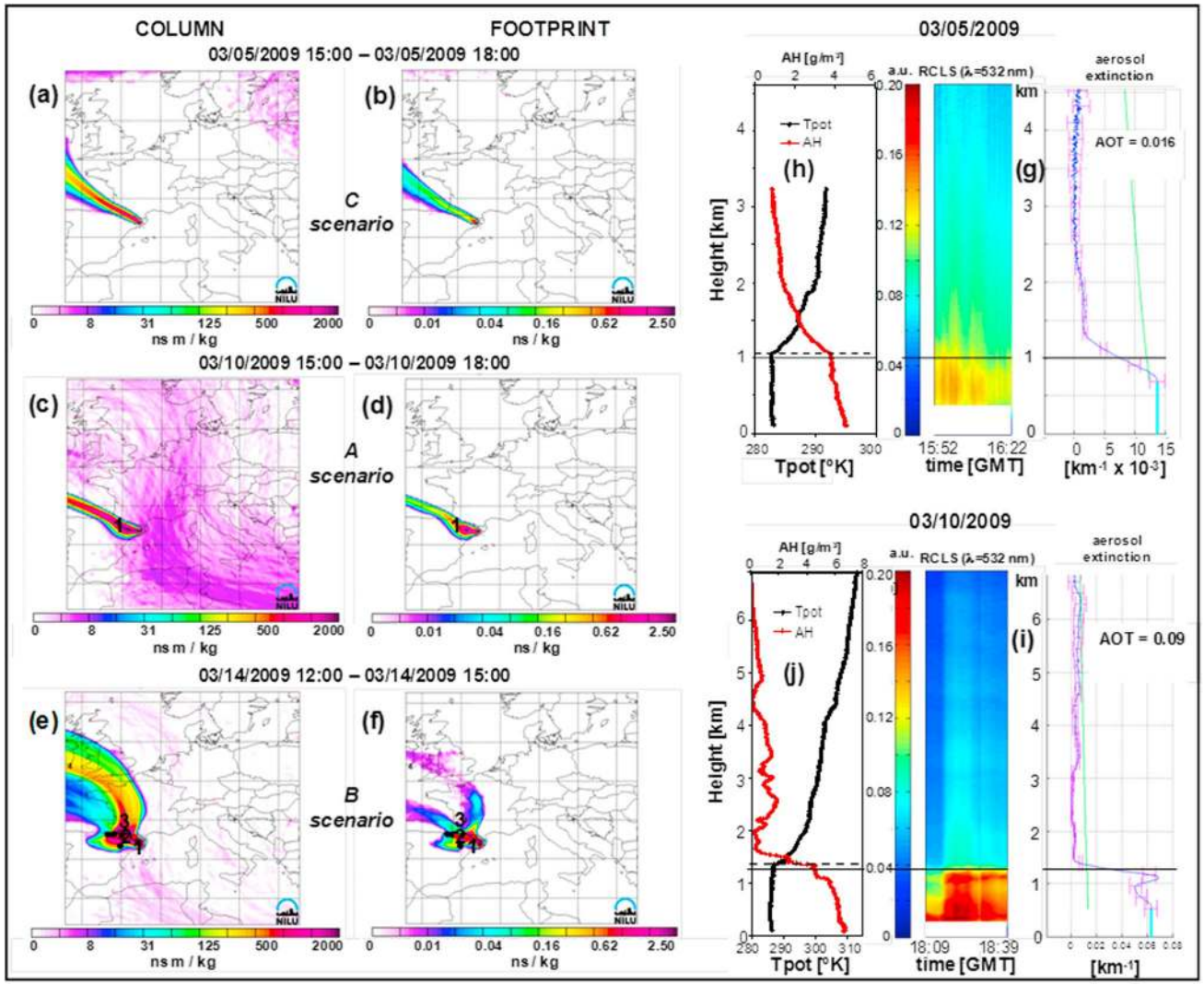

Figure 9. (a–f) FLEXPART column integrated and footprint emission sensitivities for MSY (upper/lower release height 720 m) calculated on 5 March (15:00–18:00 GMT), 10 March (15:00–18:00 GMT), and 14 March (12:00–15:00 GMT); numbers within FLEXPART maps indicate the location of the air masses in number of days before arriving at the measurement site; range-corrected lidar signal (RCLS) and aerosol extinction vertical profile from lidar measurement performed at BCN on (g) 5 March (15:52–16:22 GMT) and (i) 3 March (18:08–18:39 GMT) with horizontal line indicating MLH from lidar; vertical profiles of potential temperature (Tpot) and absolute humidity (AH) from radiosounding launched at BCN on (h) 5 March and (j) 10 March at 12:00 GMT with horizontal dotted lines indicating MLH from radiosounding.

The pollutants accumulated during the B episode were transported to MSY as the PBL height increased during the second A episode (28 February), causing the PM_1 concentrations at MSY to reach their highest value during DAURE-W (Figure 5i). The back trajectories in Figure 8 show that air was still pretty stagnant during the two periods shown, residing for 2–3 days over the Mediterranean Sea before arriving to the MSY station. On 28 February (Figures 8a and 8b), the relatively cleaner air mass advected to MSY, leading to the observed reduction in PM1 concentrations at BCN while pollutants were rapidly transported to the regional background site.

Before 2 March (during the transition period) the air mass resided for 2 days over the area under study causing pollutant accumulation and the observed increase in PM_1 concentrations at both stations (Figures 5i, 8c, and 8d). The lidar measurement on 2 March (Figure 8e) showed a stratified atmosphere with a high AOT of 0.37 from the presence of high aerosol load within the PBL and several aerosol layers above it due to the recirculation of regional aerosols driven by the diurnal cycling of the land-sea breeze pattern. The aerosol extinction close to the ground was about 0.3 km^{-1}, higher than the value of about 0.17 km^{-1} measured on 26 February (Figure 7g).

Starting from about 5 March the North Atlantic advection scenario (Figures 9a and 9b) caused the decrease observed in the concentrations of PM1 at both stations (Figure 5) and of AOT from lidar (0.016; Figure 9g).

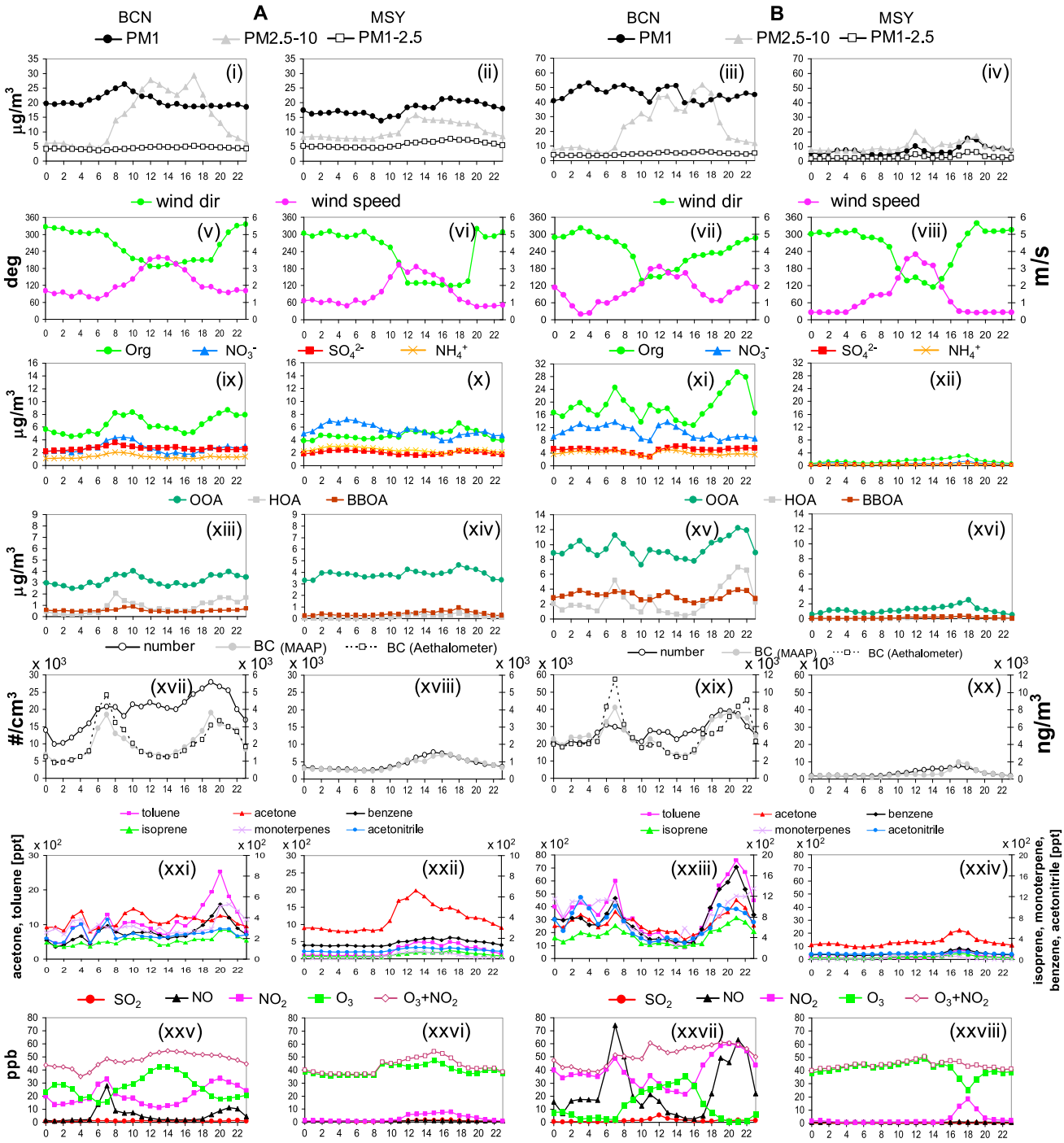

Figure 10. (i–xxviii) Mean diurnal cycles during the A and B scenarios for (left) BCN and (right) MSY.

Both lidar and radiosounding (Figure 9h) detected the MLH at about 1 km. In the subsequent long-duration A episode (8–12 March, cf. Figure 5), the PM1 concentrations started to increase again with time. The air mass was transported relatively fast from the northwest at the beginning of this A episode on 10 March (Figures 9c and 9d). The lidar measurement of 10 March (Figure 9i) measured an AOT of 0.09 and a high PBL height (around 1300 m) confirmed by radiosonde data (Figure 9j). The aerosol extinction close to the ground was 0.06 km^{-1} consistent with relatively low PM_1 levels at BCN the same day (Figure 5i). Pollutants had less time to accumulate in the air mass, thus explaining the reduction in PM1 at both BCN and MSY compared to the previous A and B episodes. Then the accumulation of pollution increased with time until the strong

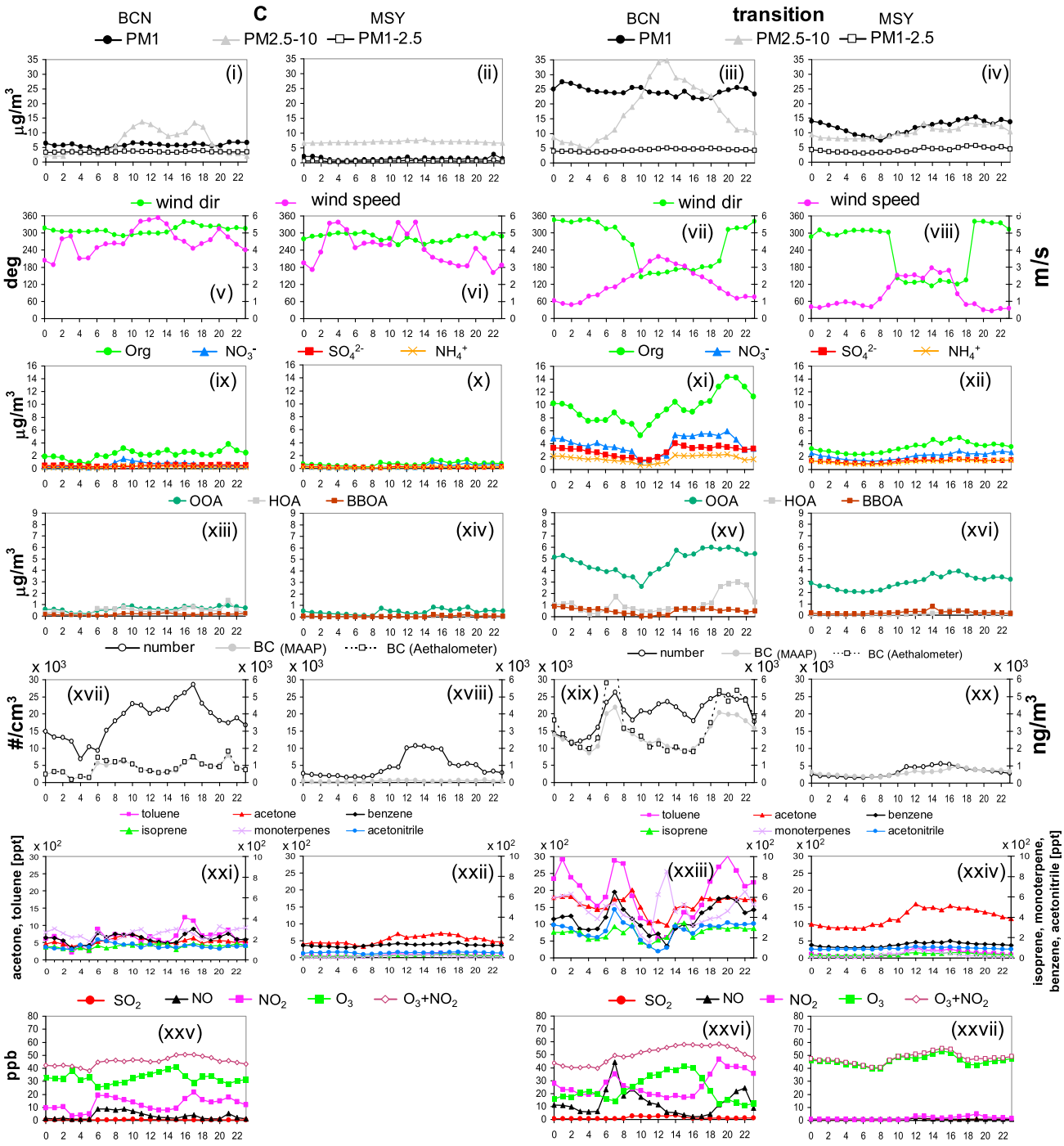

Figure 11. (i–xxvii) Mean diurnal cycles during the C and transition scenarios for (left) BCN and (right) MSY.

anticyclonic atmospheric conditions characterizing the second B episode on 14 March, with the air mass residing over the area for 3 days with subsequent accumulation of pollutants (cf. Figures 9e and 9f).

During the first half of DAURE-W (26 February to 14 March), a degree of periodicity was observed with the two B episodes preceded and followed by A episodes and with an Atlantic advection (C scenario) between the two A-B pairs. Conversely, during the second half of the campaign, no B and C episodes were observed. This period was mainly characterized by generally lower accumulation of PM with each air mass showing on average ~1 day of recirculation over the WMB (not shown). Also, the measured wind speeds and solar

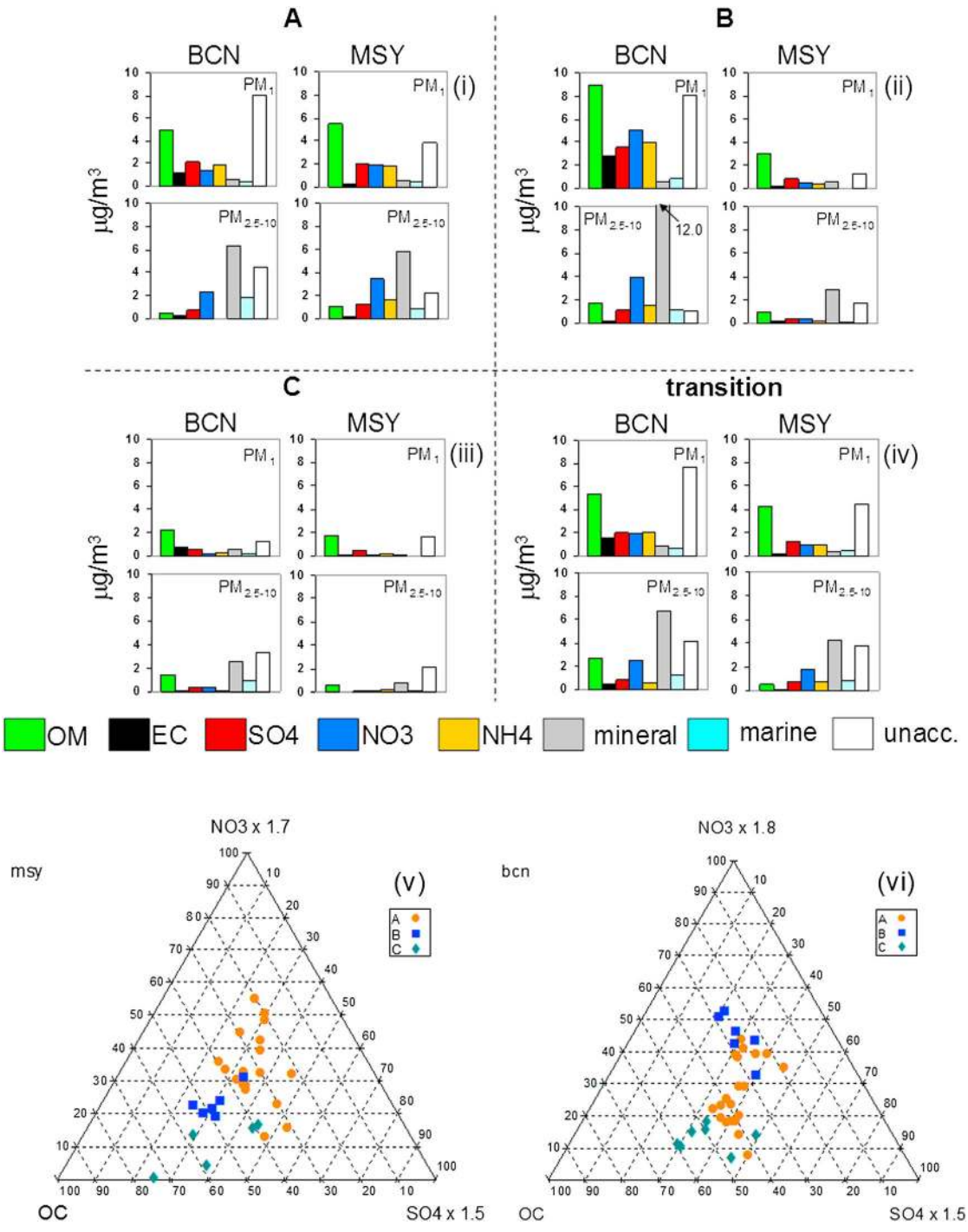

Figure 12. Main PM_1 and $PM_{2.5–10}$ chemical components averaged over the (i) A scenarios, (ii) B scenarios, (iii) C scenarios, and (iv) transition scenarios. Three-component diagrams comparing OC, NO_3^-, and SO_4^{2-} concentrations during the A, B, and C scenarios at (v) MSY and (vi) BCN. SO_4^{2-} and NO_3^- concentrations were adjusted to place the abundances of the three elements in the center of the triangle.

radiation showed an increase toward the end of the campaign together with a general reduction of PM_1 concentrations at both BCN and MSY (starting from 20 March).

3.2.3. PM Diurnal Cycles and Chemistry

The role of the mesoscale circulations on PM dynamics in the WMB is analyzed in this section by investigating the diurnal cycles of some key atmospheric chemical components measured during DAURE-W. Figures 10 and 11 show the diurnal cycles of PM and gas phase components for BCN and MSY under scenarios A and B

(Figure 10) and C and transition (Figure 11). Figure 12 shows the concentrations by scenarios of the main PM_1 and $PM_{2.5-10}$ chemical components during DAURE-W from the analysis of the 12 h filters. Mean concentrations for each scenario are reported in the supporting information.

3.2.3.1. A Scenarios

Under the A scenarios, the concentrations of PM_1 at MSY (Figure 10ii) had a diurnal cycle driven by the sea breeze which developed from about 10:00 GMT to 19:00 GMT coming from the southwest and transporting pollutants from the coastal region toward MSY (Figure 10vi). Development of a sea breeze led to steady winds (3–4 m/s) transporting pollutants inland, causing the observed increase in the concentrations of PM_1 at MSY. At MSY PM_1 concentrations reached 21 $\mu g/m^3$ around 16:00–18:00 GMT (from around 17 $\mu g/m^3$ in the morning), while lower PM_1 concentrations were simultaneously measured at BCN. In BCN the increase of the diurnal PBL height in combination with the cleaning effect of the sea breeze caused the decrease of PM_1 concentrations from a morning peak of ~25 $\mu g/m^3$ to ~18 $\mu g/m^3$ around 16:00–18:00 GMT (Figure 10i). During the night (22:00–05:00 GMT), fairly constant PM_1 concentrations around 17 and 20 $\mu g/m^3$ were measured at MSY and BCN, respectively. The presence of residual pollution within the relatively high PBL at night coupled with low wind conditions explained the high PM_1 concentrations observed on regional scales at night.

The concentration of SO_4^{2-} from the HR-AMS at both sites was similar (2.0 and 2.7 $\mu g/m^3$ at MSY and BCN, respectively; cf. Table S3) due to its more regional nature [*Querol et al*., 2008b]. However, the mean NO_3^- concentrations at MSY from HR-AMS (5.5 $\mu g/m^3$) were double those measured at BCN (2.7 $\mu g/m^3$) likely due to the lower ratio temperature/relative humidity (T/RH; cf. Table S1) at MSY and the formation of NO_3^- during the transport of air masses toward MSY station. Filter analysis in Figures 12i, 12v, and 12vi showed that the concentrations of fine and coarse NO_3^- were higher at MSY than in BCN during the A scenario, with a mean MSY/BCN NO_3^- ratio from PM1 filters around 1.4. Moreover, similar concentrations of fine and coarse SO_4^{2-} and organic matter (OM) from filters were measured at both stations.

On average, concentrations of NR-PM1 from the HR-AMS of 14.9 $\mu g/m^3$ (32% OA, 67% SIA) and 13.4 $\mu g/m^3$ (48% OA, 50% SIA) were measured at MSY and BCN, respectively, during the A scenario. Similar concentrations of OOA were measured at MSY (3.9 $\mu g/m^3$, 83% of OA) and BCN (3.2 $\mu g/m^3$, 49% of OA), indicating the regional nature of SOA, consistent with previous studies [e.g., *Zhang et al*., 2007]. The HOA concentrations from PMF analysis were instead much higher at BCN (0.9 $\mu g/m^3$, 14% of OA) compared with MSY (0.2 $\mu g/m^3$, 4% of OA) mainly due to traffic emissions. Similarly, the mean EC concentration from filters was higher at BCN (~1.2 $\mu g/m^3$) compared with MSY (~0.3 $\mu g/m^3$) (cf. Figure 12i). At BCN the diurnal cycles of NO_3^- and HOA were similar to that of PM1 with peaks around 7:00–9:00 and 19:00–21:00 GMT corresponding to the busiest traffic of the day within the city [*Amato et al*., 2009b] (Figure 10ix). Traffic-related increases in black carbon concentration (BC; Figure 10xvii), toluene and benzene (Figure 10xxi), and NO and NO_2 (Figure 10xxv) were also observed. The concentrations of acetonitrile which is usually used as a tracer for biomass burning [*Bange and Williams*, 2000] increased during rush hours in BCN, suggesting contribution from fossil fuel combustion during these peaks [*Seco et al*., 2013].

Relatively low and similar BBOA concentrations (around 0.4–0.5 $\mu g/m^3$) were measured at both stations (Figures 10xiii and 10xiv), while VOC mixing ratios were higher at BCN with the exception of acetone which showed similar concentrations (around 1.1–1.2 ppbv) (Figures 10xxi and 10xxii). As reported in *Seco et al*. [2011], the polluted air masses reach the MSY site after passing over urban and industrial areas surrounding the Barcelona metropolitan area, where they were enriched in VOCs of biogenic and anthropogenic origin causing the observed increase in VOCs concentrations in the afternoon.

The mean value of the toluene/benzene ratio during the A scenario was 4.0 ± 2.0 and 1.4 ± 1.0 at BCN and MSY, respectively, indicating the presence of fresher vehicular emissions at BCN compared to those at MSY [*Cubison et al*., 2006]. At BCN the values of the toluene/benzene ratio did not show a marked diurnal cycle (not shown), while at MSY the higher ratios (toluene/benzene = 2.0) were observed in late morning through the whole afternoon compared with night-early morning (toluene/benzene = 0.8) likely due to the transport of fresher vehicular emissions advected by the sea breeze.

The diurnal cycle of coarse PM ($PM_{2.5-10}$) at BCN had a large diurnal cycle with night lows (6 $\mu g/m^3$) and daytime highs (25–29 $\mu g/m^3$) (Figure 10i). Construction and traffic-induced resuspension are thought to be responsible for the observed diurnal cycles of the $PM_{2.5-10}$ fraction at BCN [*Reche et al*., 2011a; *Amato et al*., 2009b] like in other

areas [*Barmpadimos et al.*, 2011]. Both processes mainly emit coarse particles during the busiest traffic and construction hours within the city. Figure 12i shows that the main component of the $PM_{2.5–10}$ fraction at BCN was mineral matter followed by the unaccounted part. Continuous emission of coarse particles is needed to sustain the high $PM_{2.5–10}$ concentrations because of the simultaneous cleansing effect of the breeze. The importance of traffic resuspension of PM in urban environments has been discussed elsewhere [e.g., *Thorpe and Harrison*, 2008; *Amato et al.*, 2009a; *Bukowiecki et al.*, 2010]. At MSY the coarse PM2.5–10 concentrations, mainly consisting of mineral matter, followed by secondary nitrate particles (cf. Figure 12i), showed a different diurnal cycle driven by the sea breeze circulation with concentrations increasing from late morning through the afternoon followed by a decrease from 19–24 h to almost constant levels during the night and midmorning (Figure 10ii).

3.2.3.2. B Scenarios

Under the B scenarios, the effect of the strong inversion at BCN led to an accumulation of PM_1 concentration, on average high throughout the day, reaching values higher than 50 $\mu g/m^3$ and showing a slight decreasing trend starting from 14:00 GMT when the sea breeze was fully developed (Figure 10iii). Under these atmospheric conditions the sea breeze showed a reduced effect in cleaning the urban site. Compared with the A scenario, the primary tracers of traffic emissions, such as BC (Figure 10xix), aromatic VOCs (Figure 10xiii), NO, NO_2 (Figure 10xvii), and HOA (Figure 10xv), showed a more distinct and greater morning and evening peak under the B scenario in BCN. Secondary aerosol species such as OOA (Figure 10xv), SO_4^{2-}, and NO_3^- (Figure 10xi) did not show a clear morning peak as during the A scenario. The low O_3 levels measured at BCN during the B scenario were due to the strong titration by the high NO concentrations (Figure 10xxvii).

Under B scenarios the concentrations of all reported chemical components were strongly elevated in the fine mode at BCN compared with the other scenarios, with the highest concentrations of OM, EC, and SIA measured during DAURE-W (Figure 12ii). The coarse mode at BCN mainly showed high concentrations in crustal material and secondary nitrate. Figures 12v and 12vi show that the highest differences between BCN and MSY in the relative contributions of OC, SO_4^{2-}, and NO_3^- to PM1 were observed under the B scenario compared with A and C scenarios. The relative contribution from NO_3^- was high in BCN, whereas the relative contribution from organics was higher at MSY compared with BCN.

Mean NR-PM_1 concentrations at BCN were 39.5 $\mu g/m^3$ with relative fractions of NR species (48% OA, 50% SIA) similar to those under the A scenario. PMF analysis resolved OOA, HOA and BBOA as 50%, 14% and 17% of OA mass, respectively, at BCN during the B scenarios, in agreement with the values reported from *Mohr et al.* [2012] for the entire DAURE-W campaign. At MSY average NR-PM_1 concentrations were only 2.6 $\mu g/m^3$ (52% OA, 48% SIA), due to its location above the inversion. Multiple pollutants showed an increasing trend from around 15:00 until 19:00 GMT at MSY likely due to transport of pollutants by the sea breeze.

The concentrations of VOCs at BCN under the B scenario were the highest measured during DAURE-W with mixing ratios higher than at MSY by factors ranging from 2 for acetone up to 25 for monoterpenes (cf. Table S3). At MSY the concentrations of the biogenic isoprenoids (monoterpenes and isoprenes) and acetone were similar to those measured under the A scenario. Toluene and benzene at MSY were around 50% higher under the A scenario compared with the B scenario. High ambient air temperature and solar radiation and calm winds observed under the B scenario (Table S1) may explain the similar concentrations of isoprenoid VOCs at MSY under A and B scenarios. Also, acetonitrile concentrations were similar for the A and B scenarios at MSY, while toluene, benzene, NO_x, and BC were lower under the B scenario compared with those under A (by around 50, 50, 30, and 70%, respectively) as a consequence of the location of the MSY station above the inversion.

Mean toluene/benzene ratios under the B scenario (4.6 ± 1.2 and 1.4 ± 1.0 at BCN and MSY, respectively), were similar to those measured under the A scenario. As reported in Figure 10, local emissions at MSY caused a slight increase in pollutants around 17:00 GMT (Figures 10iv, 10xii, 10xx, and 10xxiv). The local origin of these pollutants is demonstrated by the cessation of the sea breeze and the reduction in wind speed at 17:00 at MSY (Figure 10viii). These conditions do not allow the transport of pollutants from the Barcelona metropolitan areas and industrialized valleys toward MSY. The mean toluene/benzene ratio around 17:00 GMT at MSY under the B scenario was around 3.5. After excluding the data around 17:00, the toluene/benzene ratio at MSY dropped to a mean value of around 1.2 due to the position of the MSY station in the more aged free troposphere. Finally, under the B scenario the mean BBOA concentration at BCN was greater than 3 $\mu g/m^3$ compared with 0.1 $\mu g/m^3$ measured at MSY probably due do the decoupling of MSY from boundary layer biomass burning sources.

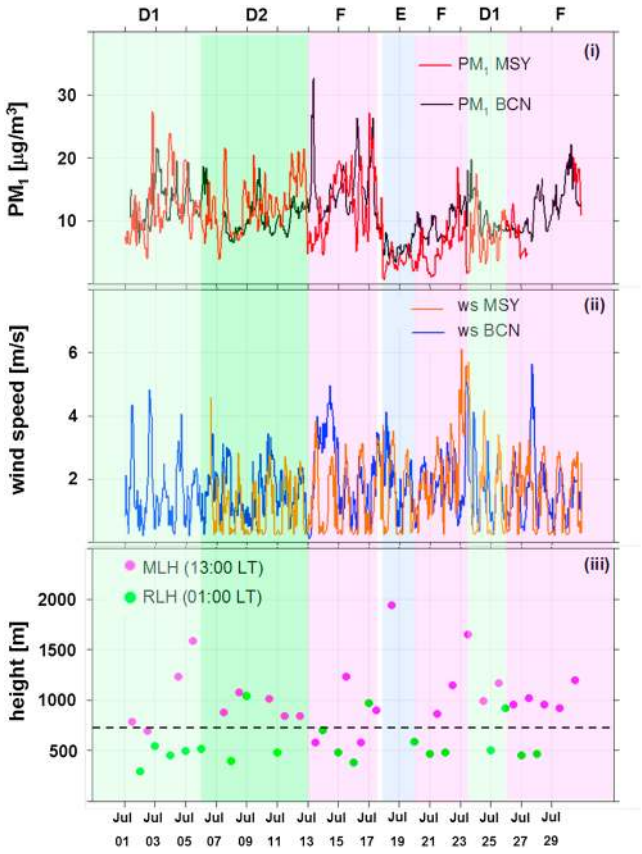

Figure 13. (i) PM_1 Grimm corrected mass concentration levels at BCN and MSY, (ii) wind velocity at BCN and MSY, and (iii) PBL heights over BCN.

3.2.3.3. C Scenario

Under the C scenario winds came constantly from the west with relatively high speeds (> 4 m/s; cf. Figures 11v and 11vi) cleaning the atmosphere, and the lowest PM_1 concentrations were observed at both measurement sites (Figures 10i and 10ii). Also, the mean NR-PM_1 concentrations at BCN (3.5 μg/m^3, 62.1% OA, 36.6% SIA) and at MSY (1.5 μg/m^3, 47.7% OA, 51.0% SIA) were the lowest registered during DAURE. The relative contributions to PM_1 of OC, NO_3^-, and SO_4^{2-} was similar at both stations with reduced relative contributions from NO_3^- at both BCN and MSY (Figures 12v and 12vi). Interestingly, O_3 and particle number concentration were similar to those during A scenarios. For the former this may indicate that O_3 is largely controlled by the Northern Hemisphere background rather than photochemical production during winter and for the latter condensation or increased new particle formation due to reduced aerosol surface area. The lowest mean toluene/benzene ratios of 2.8 ± 1.4 and 0.5 ± 0.4 at BCN and MSY, respectively, were measured under the C scenario indicating less fresh vehicular emissions compared with A and B scenarios at both sites.

3.3. DAURE Summer Campaign

The aerosol composition data obtained for the summer DAURE campaign was less comprehensive than the data obtained during the winter campaign. For example, during the summer DAURE campaign high-resolution data from HR-AMS were not available, while PTRMS data were available for 4 days during the period 25 July to 10 August at MSY and for 5 days during 16–24 July at BCN. However, measurements/modeling from many groups reported in Table 1 were replicated during the summer campaign, thus allowing a good comparison of the summer and winter aerosol phenomenology.

3.3.1. PM_1 Scenarios

Figure 13 shows the concentrations of PM_1 (Figure 13i), wind speed (Figure 13ii), and PBL heights (Figure 13iii) measured at BCN and MSY during DAURE-S. Mean concentrations of PM_1 during DAURE-S were 12 ± 4 μg/m^3 at BCN and 11 ± 5 μg/m^3 at MSY (Table S5 in supporting information). These summer concentrations were around 50% and 20% lower than the levels measured during DAURE-W at BCN and MSY, respectively. An important difference was observed by comparing the summer (Figure 13i) and winter (Figure 5i) PM_1 time series. PM_1 concentrations at MSY and BCN during summer were always similar, mainly as a consequence of the lack of the strong inversions commonly observed in winter which led to the clear decoupling between BCN and MSY stations. This difference demonstrates the potential of the strong winter pollution episodes in increasing the fine PM concentrations at BCN during winter and the higher dispersion of pollutants within the higher PBL heights in summer. During DAURE-S, MSY was always within the PBL at 12:00 GMT due to strong summertime diurnal convection. On the contrary, during the night MSY was on average above the PBL. As shown in the next paragraph, the presence of aerosol layers above the PBL from summertime recirculation explained the high concentrations of PM_1 measured at MSY during the day.

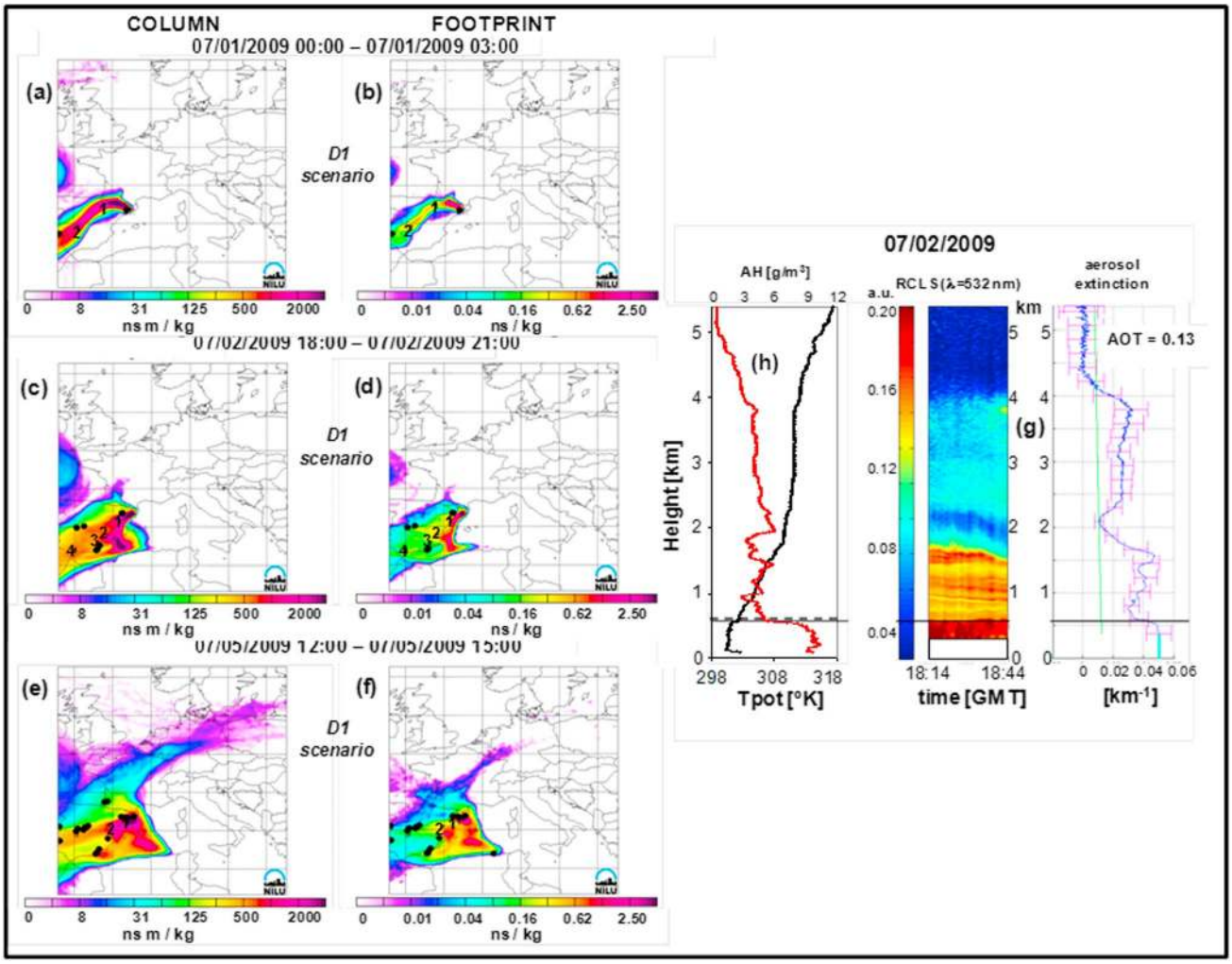

Figure 14. (a–f) FLEXPART column integrated (left) and footprint emission sensitivities (right) for MSY (upper/lower release height 720 m) calculated during the first D1 episode on 1 July (00:00–03:00 GMT), 2 July (18:00–21:00 GMT), and 5 July (12:00–15:00 GMT); numbers within FLEXPART maps indicate the location of the air masses in number of days before arriving at the measurement site; (g) range-corrected lidar signal (RCLS) and aerosol extinction vertical profile from lidar measurement performed at BCN on 2 July from 18:14 to 18:44 GMT with horizontal line indicating MLH from lidar; (h) vertical profiles of potential temperature (Tpot) and absolute humidity (AH) from radiosounding launched at BCN on 2 July at 12:00 GMT with horizontal dotted line indicating mixing layer height (MLH) from radiosounding.

3.3.2. Meteorological Scenarios

Due to the similarity between the PM_1 concentrations observed at BCN and MSY during DAURE-S, the different scenarios were defined by using the FLEXPART back trajectories. During the first 2 weeks of the campaign (01–13 July) a typical summer regional recirculation scenario was observed (D1 and D2 scenarios in Figure 13). Under the D1 scenario (01–07 July) the air masses came from the central/southern part of the Iberian Peninsula (Figures 14a–14f), while the air masses passed over the north of Spain under the D2 scenario (07–13 July; Figure 15). In both cases, air masses showed at least 2 days of accumulation, over the coastline in the first case (D1) and over Northern Spain in the second case (D2). The lidar measurement performed on 02 July from 18:14 to 18:44 GMT (Figure 14g) showed the presence of aerosol layers with different aerosol loadings above the PBL (located at around 700 m; cf. Figures 14g and 14h) up to an altitude of about 4.5 km leading to an AOT of 0.13. These layers formed from regional recirculation of polluted air masses. No lidar measurements were available over the D2 scenario.

Three separate African dust events (F scenarios) were observed during DAURE-S for a total of 14 days, while no major African dust outbreaks were registered during the winter period [*Jorba et al.*, 2013].

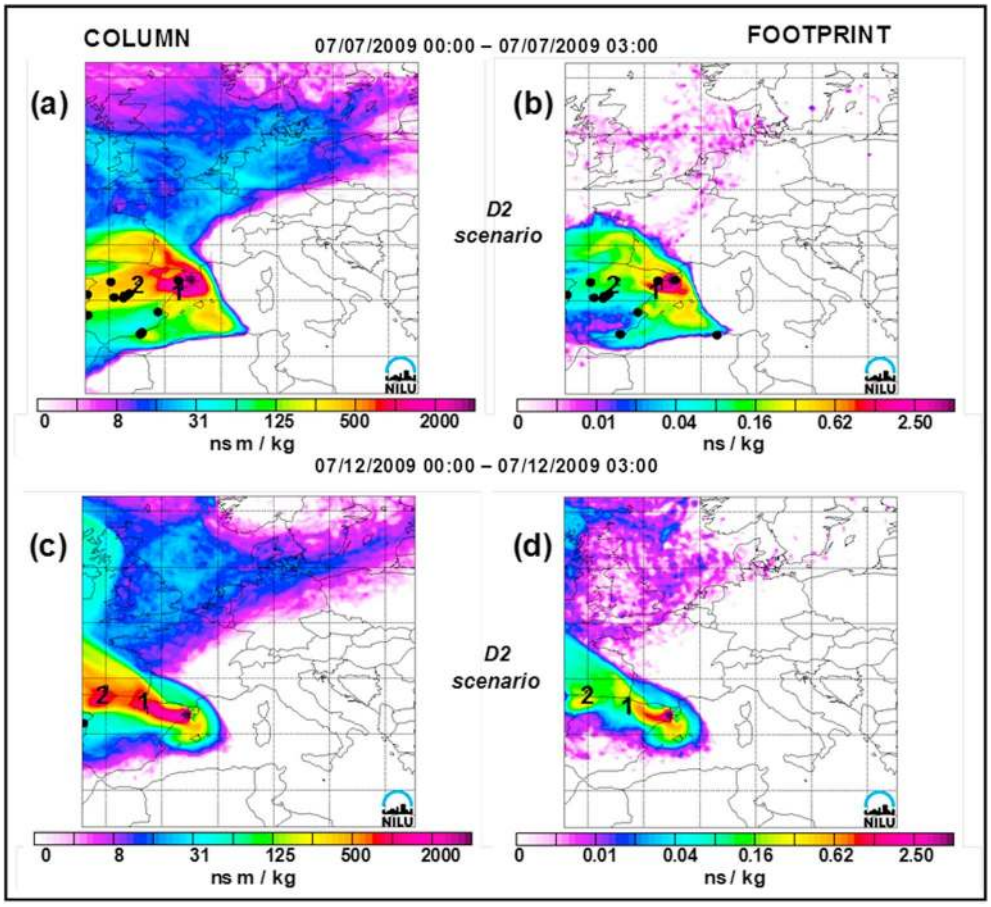

Figure 15. (a–d) FLEXPART column integrated (left) and footprint emission sensitivities (right) for MSY (upper/lower release height 720 m) calculated during the D2 episode on 7 July (00:00–03:00 GMT) and 12 July (00:00–03:00 GMT); numbers within FLEXPART maps indicate the location of the air masses in number of days before arriving at the measurement site.

Figure 16 shows the FLEXPART back trajectories calculated on 13 July (Figures 16a and 16b) and 17 July (Figures 16c and 16d) during Saharan dust outbreaks. The lidar measurements performed on 13 July around 12:00 GMT (Figure 16g) showed a strong aerosol layer in the free troposphere between 1.7 and 4 km related to dust transport from Africa. Dry deposition of Saharan dust within the PBL caused the mean PM_1/PM_{10} ratio at MSY site (0.4 ± 0.1) to be lower than during D1 and D2 scenarios (0.6 ± 0.1) indicating higher concentration of fine particles under regional episodes and higher concentrations of coarse particles under F scenarios. On 13 July the AOT was 0.18, higher than the AOT measured by lidar under D1 (Figure 14g). The E episode was characterized by air masses coming relatively fast from the West as evidenced by FLEXPART back trajectories for 19 July (Figures 16e and 16f). However, the wind velocity measured during the E scenario at both BCN and MSY did not show an increase compared to the D1, D2, and F scenarios, and it was much lower than the mean wind velocity measured during the Atlantic advection episode observed during DAURE-W (cf. Tables S1 and S2). Nevertheless, the lowest PM_1 concentrations (5.6 $\mu g/m^3$ at BCN and 4.6 $\mu g/m^3$ at MSY) and AOT (0.08; Figure 16g) were measured during the E scenario attributable to the origin of the air masses over the Atlantic Ocean.

3.3.3. PM Diurnal Cycles and Chemistry

Figures 17 and 18 show the diurnal cycles of PM_x, wind direction and speed, particle number concentration, BC, and gaseous pollutants grouped by the different scenarios observed during DAURE-S. The average concentrations of the main PM_1 and $PM_{2.5-10}$ chemical components from filters analyses separated by the four observed summer scenarios are reported in Figure 19. For the D1 scenario (Figure 19i), only the $PM_{2.5}$ fraction was reported as no PM_1 measurements were available for the MSY station during the first week of the campaign.

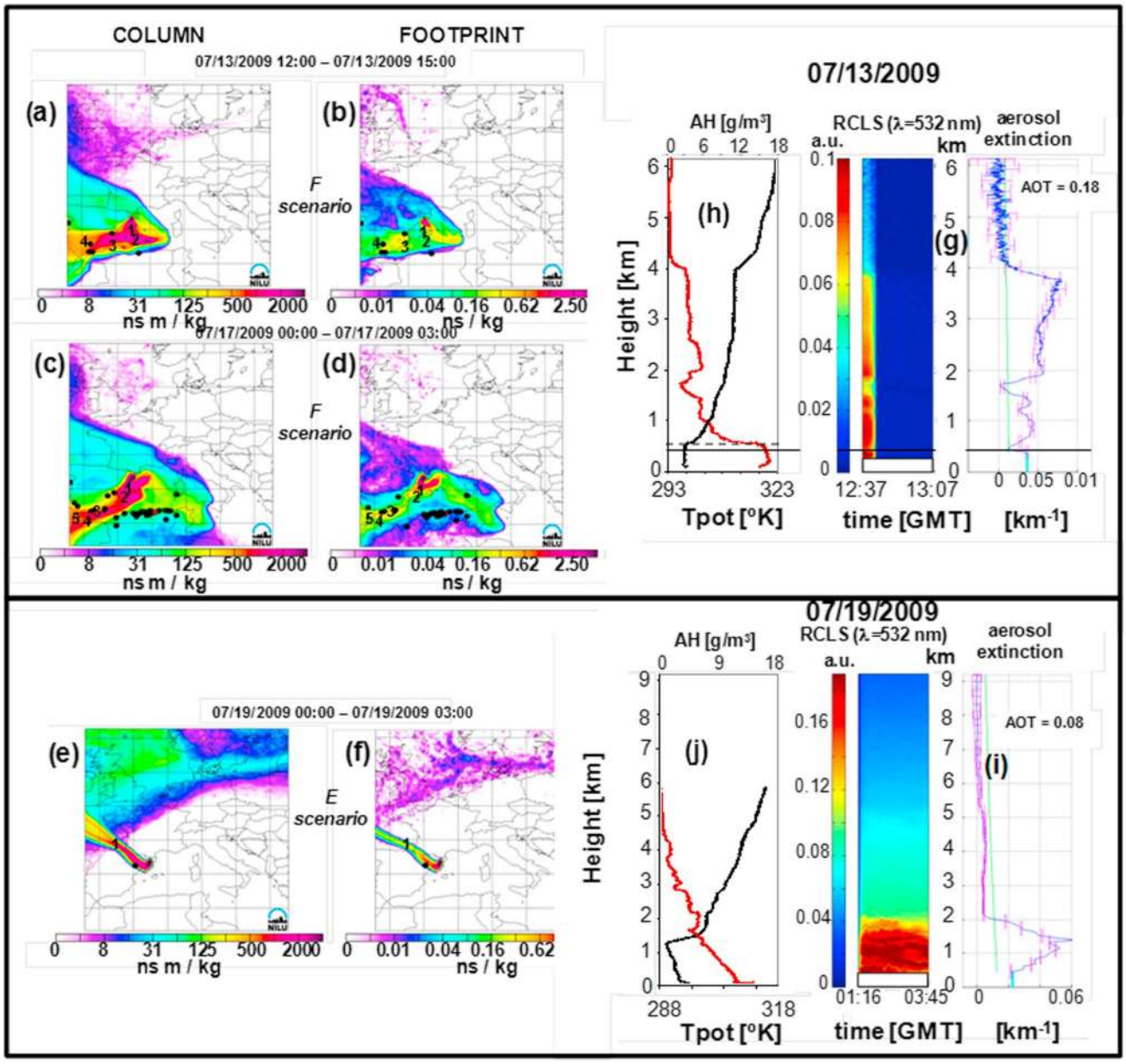

Figure 16. (a–f) FLEXPART column integrated (left) and footprint emission sensitivities (right) for MSY (upper/lower release height 720 m) calculated during the first F episode on 13 July (12:00–15:00 GMT) and 17 July (00:00–13:00 GMT) and during the E episode on 19 July (00:00–03:00 GMT); numbers within FLEXPART maps indicate the location of the air masses in number of days before arriving at the measurement site; range-corrected lidar signal (RCLS) and aerosol extinction vertical profile from lidar measurement performed at BCN (g) on 13 July from 12:07 to 12:37 GMT and (i) on 19 July from 01:16 to 03:46 GMT with horizontal line indicating MLH from lidar; vertical profiles of potential temperature (Tpot) and absolute humidity (AH) from radiosounding launched at BCN on (h) 13 July and (i) 19 July at 12:00 GMT with horizontal dotted line indicating mixing layer height (MLH) from radiosounding.

In summer the PM diurnal cycles showed some similar characteristics to those observed in winter. In general, the land-sea breezes played an important role in modulating the PM_1 concentrations at MSY (Figures 17ii, 17iv, 18ii, and 18iv). The effect of the sea breeze also caused the increase observed in the afternoon for BC concentrations at MSY (Figures 17ix, 17xi, 18x, and 18xii). At the BCN site, the diurnal variation of the PM_1 concentrations in summer was less pronounced than in winter and mainly during the D1 and D2 scenarios. This was due to the higher dispersion of pollutants within the PBL and the presence of relatively more polluted air masses over the sea in summer due to the recirculation [*Millán et al.*, 1997; *Rodriguez et al.*, 2003], leading to a reduced cleansing effect of the breeze over the coastal site.

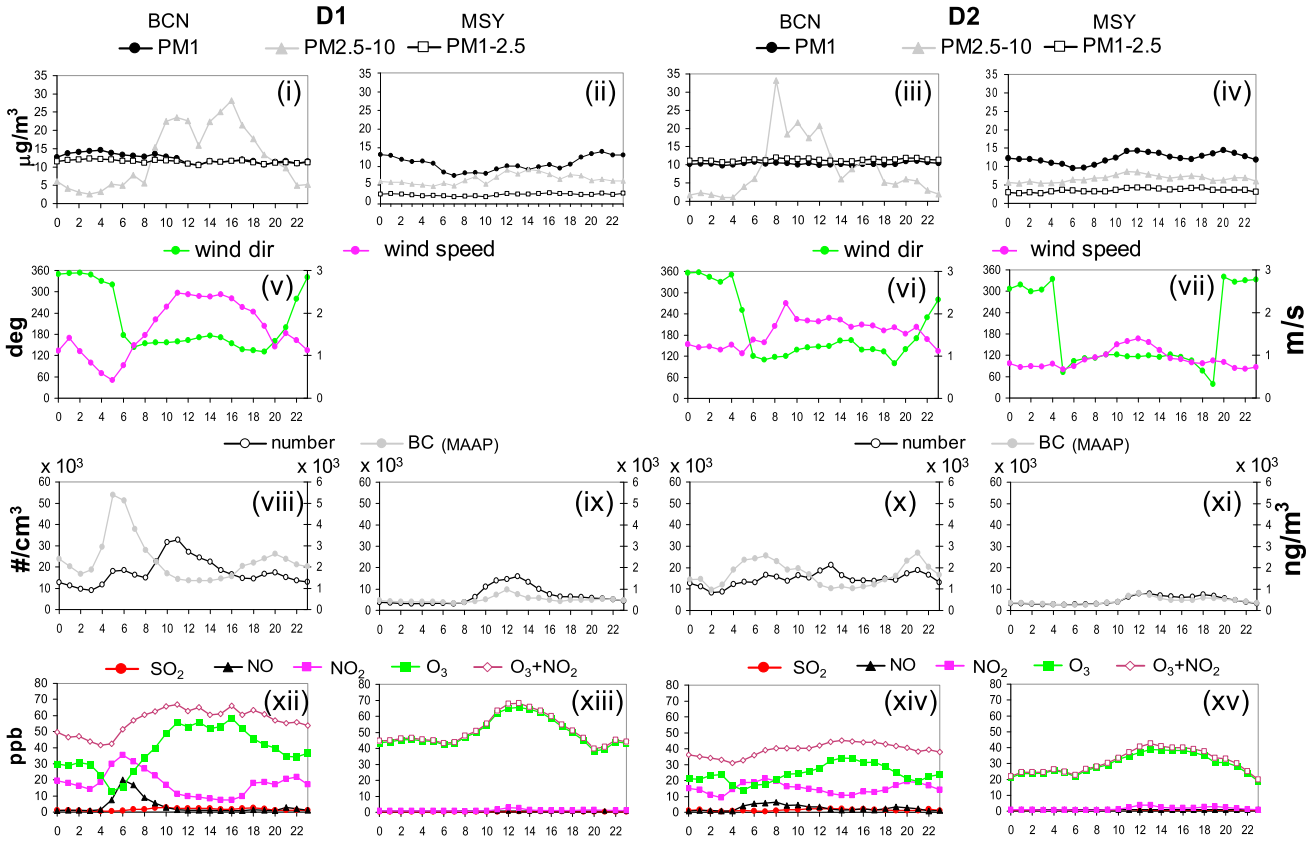

Figure 17. (i–xv) Mean diurnal cycles during the summer D1 and D2 scenarios for BCN (left) and MSY (right).

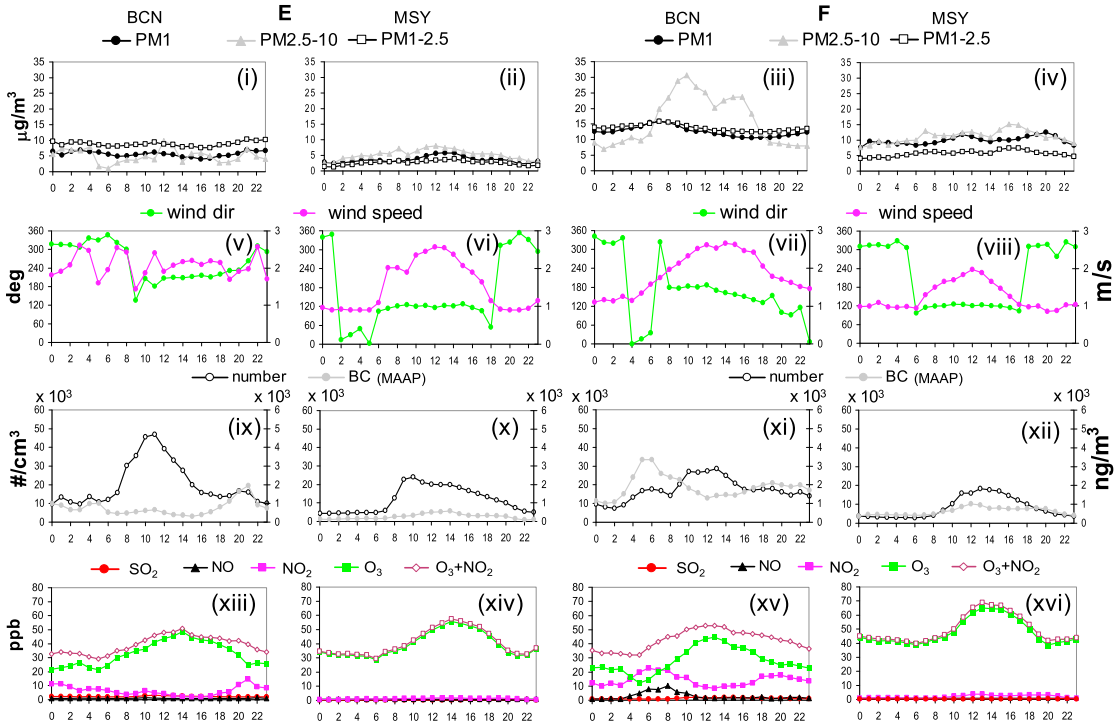

Figure 18. (i–xvi) Mean diurnal cycles during the summer E and F scenarios for BCN (left) and MSY (right).

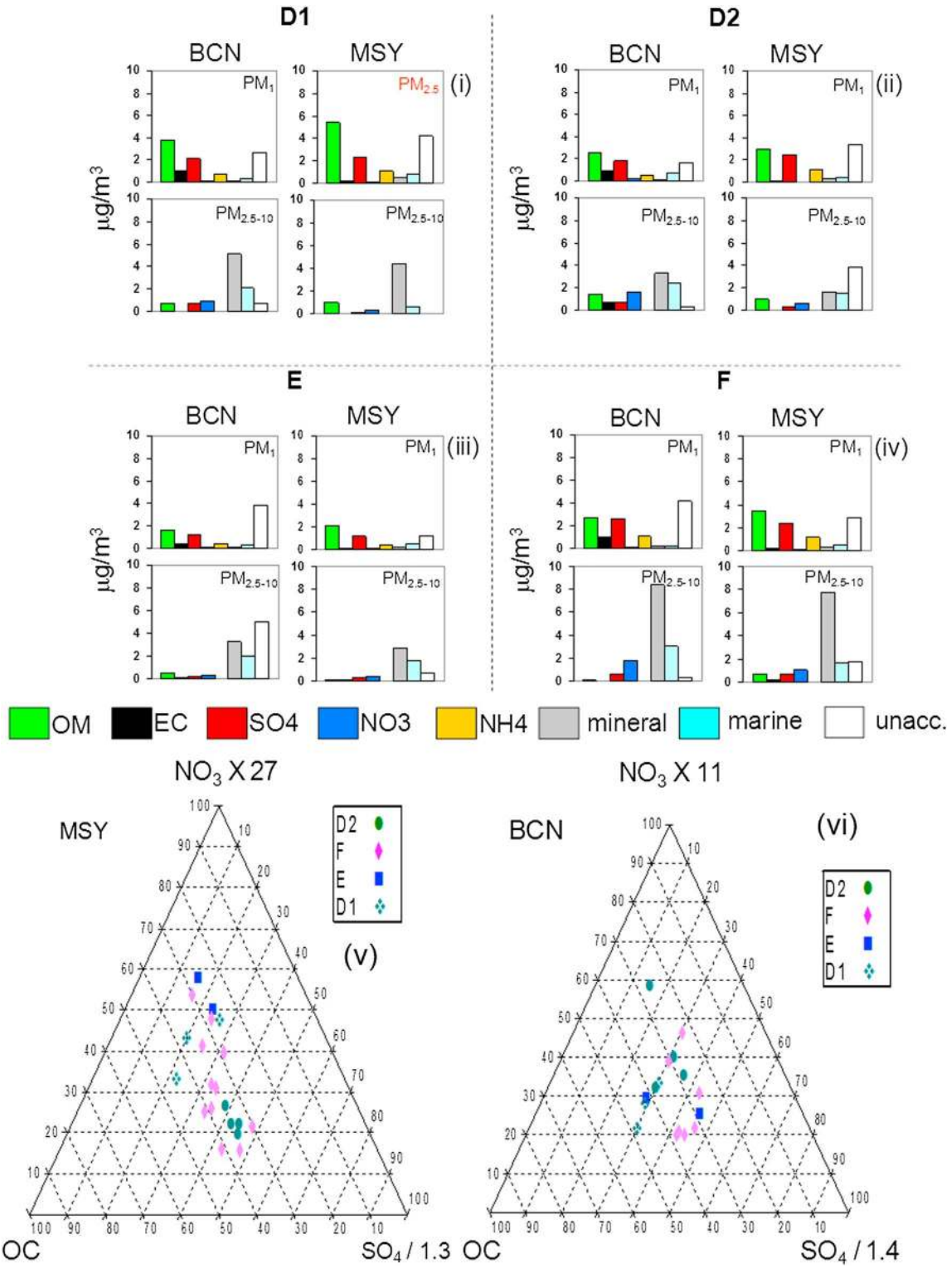

Figure 19. Main PM_1 and $PM_{2.5-10}$ chemical components averaged over the (i) D1 scenarios, (ii) D2 scenarios, (iii) E scenarios, and (iv) F scenario. Three-component diagrams comparing OC, NO_3^-, and SO_4^{2-} concentrations during the D1, D2, E, and F scenarios at (v) MSY and (vi) BCN. SO_4^{2-} and NO_3^- concentrations were adjusted to place the abundances of the three elements in the center of the triangle.

The coarse particle mode at BCN was driven by traffic resuspension and construction within the city with the highest concentrations observed during the late morning through the whole afternoon. The lowest $PM_{2.5-10}$ concentrations at BCN (around 5 $\mu g/m^3$) were measured during the E scenario as a consequence of the transport of clean air from the ocean, as demonstrated by the reduction of PM_x observed also at the MSY site, and the reduction in traffic and construction emissions at BCN given that the E scenario occurred during the weekend (Friday–Sunday). The highest coarse PM concentrations were observed at both BCN (16 $\mu g/m^3$) and MSY (11 $\mu g/m^3$) during the F episode, when air masses from Africa affected the WMB.

The particle number concentrations increased in the early morning at BCN related to traffic emissions and around midday due to nucleation episodes occurring when gaseous pollutants and particle concentrations are diluted and maximum insolation and O_3 levels occur leading to new secondary particle formation [*Reche et al*., 2011b]. As reported in the supporting information, the highest number concentration at both BCN and MSY was observed during the short advection E episode in correspondence with the cleanest atmospheric conditions favoring nucleation processes and new particle formation.

During DAURE-S the concentrations of the main chemical PM components in Figure 19 were on average similar at BCN and MSY in both the fine and coarse modes (cf. supporting information, Table S6). A difference was observed for EC concentrations which were substantially higher at BCN (around 0.9 $\mu g/m^3$ in PM1) than at MSY (0.2 $\mu g/m^3$), whereas similar OM were measured at both stations suggesting the importance of SOA formation at the regional background station. Relative contributions to PM_1 of OC, SO_4^{2-}, and NO_3^- were highly variable at both stations (Figures 19v and 19vi). At MSY a difference was observed between D1 and D2 scenarios, with SO_4^{2-} relative contributions higher during D2 than during D1, likely due to the air masses origin during D2 moved over the north of Spain. Ozone concentrations during D2 were around 40% lower compared with the mean O_3 concentrations measured during DAURE-S. Moreover, D2 was characterized by a large thunderstorm offshore the eastern coast of Spain with cumulus clouds developed during daytime producing intense precipitation events over the sea [*Jorba et al*., 2013].

The average $PM_{2.5-10}$ concentrations observed during DAURE-S (13 ± 16 $\mu g/m^3$ at BCN and 9 ± 6 $\mu g/m^3$ at MSY) were similar to the concentrations measured in winter (15 ± 17 $\mu g/m^3$ at BCN and 10 ± 5 $\mu g/m^3$ at MSY, cf. supporting information) despite the general absence of precipitation in the WMB and the high frequency of African dust transport in summer. This similarity was due to the efficiency of the observed winter pollution episodes in increasing the average PM concentrations at both BCN (B scenario) and MSY (A scenario) and the relatively low intensity of the Saharan dust episodes observed during summer.

The availability of VOCs measurements during DAURE-S at BCN and MSY was limited to two short periods (cf. supporting information, Table S5). Important differences between the two stations were observed mainly for toluene and benzene, as concentrations were lower at MSY (269 and 66 pptv, respectively) compared with those at BCN (887 and 142 pptv, respectively); for monoterpenes concentrations were much higher at MSY (679 pptv) compared to those at BCN (246 pptv). Conversely, in winter monoterpenes and also isoprene concentrations were higher at BCN compared to those at the MSY site [*Seco et al*., 2011, 2013].

The mean toluene/benzene ratios were higher at both sites during DAURE-S compared with those during DAURE-W with mean values of 6.1 ± 3.4 at BCN and 3.6 ± 1.8 at MSY (compared to 3.9 ± 1.7 and 1.1 ± 0.9 at BCN and MSY, respectively, in winter). Again, a pronounced daily cycle for the toluene/benzene ratio was observed at MSY compared with that at BCN (not shown).

The higher toluene/benzene ratio in summer may be explained by a strong evaporative and therefore temperature dependent toluene source compared with benzene which concentrations mainly result from the nonambient temperature dependent exhaust pipe emissions [*Schnitzhofer et al*., 2008]. As concluded by *Schnitzhofer et al*. [2008], this seasonal variation must be taken into account whenever this ratio is used to determine the chemical age of an air mass. Moreover, toluene has been reported to be emitted by plants in summer [i.e., *White et al*., 2009], thus likely contributing to the high toluene/benzene ratio in summer at MSY.

4. Conclusions

The DAURE campaign showed that the concentrations of PM in the WMB are strongly influenced by both local and regional emissions, as well as meteorological conditions. The densely populated areas along the

WMB coastline contribute to the aerosol load by large pollutant emissions, and atmospheric dynamics plays an important role determining the dispersion, transport, or accumulation of pollutants. During both winter and summer pollution episodes the concentrations of fine PM (PM_1) at regional level (MSY) are similar or even higher than those simultaneously measured at urban/coastal level (BCN), due to SIA and SOA formation, as well as the transport and accumulation of primary pollutants.

In winter the intensity of the pollution episodes at BCN and MSY depended mainly on the degree of recirculation of air masses (i.e., time for pollutant accumulation) over the area under study under anticyclonic atmospheric conditions (AAC) and the height of the PBL. At MSY in winter the highest PM_1 concentrations (similar or even higher than at BCN) occurred during medium AAC/high PBLs (A scenario), whereas at BCN strong AAC/low PBLs (B scenario) led to the highest concentrations of fine PM.

Higher NO_3^- concentrations, formed during the transport of air masses toward the MSY station, were measured at MSY compared with BCN under regional pollution episodes in winter (A scenario). OM concentrations were also high at MSY under these episodes. The absolute oxygenated OA concentrations were similar at MSY and BCN indicating the regional nature of SOA. Around 85% of OC at MSY was of secondary origin. The importance of fossil SOA formation at regional level was demonstrated by the higher fossil OC/EC ratio at MSY compared with BCN and the lower BCN/MSY ratio of fossil OC compared with the corresponding fossil EC ratio. Higher HOA concentrations were detected in BCN compared with MSY due to traffic emissions, whereas BBOA concentrations were similar at both sites during the A scenario. VOCs mixing ratios were always higher at BCN than at MSY during winter regional pollution episodes with the exception of acetone, which showed similar concentrations at both stations due to the importance of acetone emissions from natural sources. At MSY under A scenario a single, prolonged afternoon peak was observed for all pollutants as contaminated air transported by the sea breeze moves into the mountains with the exception of NO_3^- which showed reduced concentrations in the afternoon due to volatilization at higher temperature. In BCN the concentrations of NO_3^- and OM and of toluene, benzene, BC, and NO_2 emitted by vehicles showed diurnal cycles similar to that of PM_1 with peaks in the morning and late afternoon related to the rush hours. The concentrations of acetonitrile which is usually used as tracer for biomass burning also increased during rush hours suggesting contribution from fossil fuel during these peaks.

Under conditions of strong AAC/low PBLs (B scenario) the concentrations of PM and chemical components in BCN were the highest measured during DAURE-W. Conversely, the MSY station was above the polluted PBL, and much lower concentrations were measured compared with the A scenario. On average the concentrations of VOCs at BCN showed mixing ratios higher than at MSY. During the B scenario, a higher proportion of OA and lower proportion of SIA in PM_1 were observed at MSY compared with the A scenario due to the relative importance of OA formation from local biogenic sources when MSY is above the polluted PBL. Indeed, at MSY the concentrations of biogenic isoprenoids (monoterpenes and isoprene), acetone, and acetonitrile during the B scenario were similar to those measured during the A scenario. Conversely, toluene and benzene concentrations at MSY were around 50% lower during the B scenario than during the A scenario.

Finally, in winter the advection of Atlantic air masses (C episode) was observed between the two A-B scenario pairs leading to the dispersion of the accumulated pollution at both sites with consequent reduction of the concentrations of all pollutants. Interestingly, both number of particles and O_3 concentrations under the C episode were similar to those measured during the A scenario at both sites indicating that O_3 is largely controlled by the Northern Hemisphere background [*Schnitzhofer et al*., 2009] and that condensation or new particle formation due to reduced aerosol surface area may enhance under clean atmospheric conditions.

In summer the strong recirculation of air masses in the WMB and the lack of strong inversions observed during DAURE-W led to dilution of pollutants at BCN and their accumulation at MSY. As a result during DAURE-S the concentrations of PM_1 at MSY were similar to those measured at BCN. The MSY station was on average within the PBL at midday, due to the strong summer diurnal convection, and above the PBL at night. Nevertheless, the concentrations of PM_1 at night were comparable with those measured at BCN likely due to the presence of aerosol layers above the PBL. The lidar measurements clearly showed the presence of multiple aerosol layers above the PBL during summer recirculation. As a consequence of both the layering and enhanced SOA formation at regional level in summer, PM concentrations at MSY often peaked higher than at BCN. The main chemical PM components were on average similar at BCN and MSY during DAURE-S with higher concentrations of EC, toluene, and benzene concentrations at BCN than those at MSY due to

localized traffic emissions. However, the importance of SOA formation at the regional background station led to similar OM concentrations at both sites. Indeed, the concentrations of monoterpenes at MSY were roughly 3 times higher than those at BCN with isoprene and acetone having similar or higher concentrations at MSY compared with those at BCN. Moreover, the monoterpenes and isoprene concentrations were around 1 order of magnitude higher in summer than in winter at MSY.

During both seasons the fossil contribution to EC and OC was higher at BCN than at MSY due to higher fossil fuel combustion from traffic at urban level. In winter the nonfossil relative contribution to EC was higher than in summer at both BCN and MSY due to higher emissions from residential wood-based heating and open agricultural biomass burning. In BCN the nonfossil contribution to OC also was higher in winter than in summer, whereas at MSY the nonfossil OC was higher in summer probably due to higher contributions of biogenic emissions. The OOC was mostly nonfossil at both BCN and MSY. Cooking emissions in BCN, which accounted for 17% of OA as revealed by the PMF analysis of HR-AMS spectra, may be also responsible for the high fraction of modern carbon in BCN. BBOA contributions during both seasons estimated with different techniques (^{14}C analysis, PMF analysis of HR-AMS organic spectra, levoglucosan analysis, and PMF on offline filter PM_1 data) were consistent with correlation coefficients higher than 0.6 and were generally lower than the BBOA contribution to OC measured at similar environments in Central and Northern Europe. The relative contribution from fossil sources to OA at both BCN and MSY was comparable to the contributions observed in Central and Northern Europe. Thus, despite the lesser use of wood burning for residential heating in the area under study, the biogenic SOA from high VOCs emissions under high temperature in Spain may compensate for the differences in fossil and nonfossil OC sources.

Acknowledgments

This work is supported by the MINECO (Spanish Ministry of Economy and Competitiveness), the MAGRAMA (Spanish Ministry of Agriculture, Food Environment), and FEDER funds; by the Acción Complementaria DAURE CGL2007-30502-E/CLI, the VAMOS project CGL2010-19464/CLI, the European Union (EUSAAR RII3-CT-2006-026140, EUCAARI), and the Departament de Medi Ambient i Habitatge of the Generalitat de Catalunya. This work was partially funded by Generalitat de Catalunya 2009 SGR8D. J. Baldasano and O. Jorba were partly supported by grants CGL2010/19652, CSD2007-0050, and SEV-2011-00067 of Severo Ochoa Program, awarded by the Spanish Government. M.C. Minguillón was supported by a postdoctoral grant in the frame of Programa Nacional de Movilidad de Recursos Humanos del Plan nacional de I-D + I 2008–2011 from the Spanish Ministry of Science and Innovation and by the JAE-Doc CSIC program, cofunded by the European Social Fund (ESF). M. Pandolfi was funded by the Jae-DOC CSIC program cofunded by the European Social Fund (ESF). A. Day, A. M. Ortega, and J. L. Jimenez were partially supported by U.S. NSF grants ATM-0920940 and ATM-0919189 (from Atm. Chem. and OISE – Office of International Science and Engineering), and by DOE grant DE-SC0006035. A.M. Ortega was supported by DOE SCGF (ARRA/ORISE/ORAU) Fellowship DE-AC05-06OR23100; J. Peñuelas and R. Seco were supported by the Spanish Government projects CGL2010-17172 and Consolider Ingenio Montes CSD2008-00040, by the Catalan Government project SGR2009-458, and by a postdoctoral grant from Fundación Ramón Areces to R. Seco. Lidar measurements were supported by the 7th Framework Programme project Aerosols, Clouds, and Trace Gases Research Infrastructure Network (ACTRIS) (grant agreement 262254); by the Spanish Ministry of Science and Innovation and FEDER funds under the projects TEC2012-34575, TEC2009-09106/TEC, CGL2011-13580-E/CLI, and CGL2011-16124-E/CLI. Also acknowledged is L. Wacker (ETH Zurich) for making available the accelerator mass spectrometer MICADAS for ^{14}C measurement. The authors would also like to acknowledge NASA/Goddard Space Flight Center, SeaWIFS-NASA Project, University of Athens, Navy Research Laboratory-USA, and the Barcelona Supercomputing Centre for their contribution with TOMS maps, satellite images, SKIRON dust maps, NAAPs aerosol maps, and BSC-DREAM8b dust maps, respectively. The authors gratefully acknowledge the NOAA Air Resources Laboratory (ARL) for the provision of the HYSPLIT transport and dispersion model and/or READY website (http://www.arl.noaa.gov/ready.html)

References

Aiken, A. C., et al. (2008), O/C and OM/OC ratios of primary, secondary, and ambient organic aerosols with high-resolution time-of-flight aerosol mass spectrometry, *Environ. Sci. Technol.*, *42*, 4478–4485.

Amato, F., M. Pandolfi, A. Escrig, X. Querol, A. Alastuey, J. Pey, N. Pérez, and P. K. Hopke (2009a), Quantifying road dust resuspension in urban environment by Multilinear Engine: A comparison with PMF2, *Atmos. Environ.*, *43*, 2770–2780.

Amato, F., X. Querol, A. Alastuey, M. Pandolfi, T. Moreno, J. Gracia, and P. Rodríguez (2009b), Evaluating urban PM_{10} pollution benefit induced by street cleaning activities, *Atmos. Environ.*, *43*, 4472–4480.

Amato, F., et al. (2011), Size and time-resolved roadside enrichment of atmospheric particulate pollutants, *Atmos. Chem. Phys.*, *11*, 2917–2931.

Bae, M. S., J. J. Schauer, J. T. DeMinter, J. R. Turner, D. Smith, and R. A. Cary (2004), Validation of a semi-continuous instrument for elemental carbon and organic carbon using a thermal-optical method, *Atmos. Environ.*, *38*, 2885–2893.

Baldasano, J. M., L. P. Guereca, E. Lopez, S. Gasso, and P. Jimenez-Guerrero (2008), Development of a high-resolution (1 km x 1 km, 1 h) emission model for Spain: The high-elective resolution modelling emission system (HERMES), *Atmos. Environ.*, *42*, 7215–7233.

Bange, H. W., and J. Williams (2000), New directions: Acetonitrile in atmospheric and biogeochemical cycles, *Atmos. Environ.*, *34*, 4959–4960.

Barmpadimos, I., M. Nufer, D. C. Oderbolz, J. Keller, S. Aksoyoglu, C. Hueglin, U. Baltensperger, and A. S. H. Prevot (2011), The weekly cycle of ambient concentrations and traffic emissions of coarse (PM(10)-PM(2.5)) atmospheric particles, *Atmos. Environ.*, *45*(27), 4580–4590.

Barmpadimos, I., J. Keller, D. Oderbolz, C. Hueglin, and A. S. H. Prévôt (2012), One decade of parallel fine ($PM_{2.5}$) and coarse (PM_{10}–$PM_{2.5}$) particulate matter measurements in Europe: Trends and variability, *Atmos. Chem. Phys.*, *12*, 3189–3203, doi:10.5194/acp-12-3189-2012.

Bukowiecki, N., P. Lienemann, M. Hill, M. Furger, A. Richard, F. Amato, A. S. H. Prevot, U. Baltensperger, B. Buchmann, and R. Gehrig (2010), PM_{10} emission factors for non-exhaust particles generated by road traffic in an urban street canyon and along a freeway in Switzerland, *Atmos. Environ.*, *44*(19), 2330–2340.

Cavalli, F., M. Viana, K. E. Yttri, J. Genberg, and J.-P. Putaud (2010), Toward a standardised thermal-optical protocol for measuring atmospheric organic and elemental carbon: The EUSAAR protocol, *Atmos. Meas. Tech.*, *3*, 79–89, doi:10.5194/amt-3-79-2010.

Chen, X., and J. Z. Yu (2007), Measurement of organic mass to organic carbon ratio in ambient aerosol samples using a gravimetric technique in combination with chemical analysis, *Atmos. Environ.*, *41*, 8857–8864.

Cubison, M. J., et al. (2006), The characterisation of pollution aerosol in a changing photochemical environment, *Atmos. Chem. Phys.*, *6*, 5573–5588.

Cubison, M. J., et al. (2011), Effects of aging on organic aerosol from open biomass burning smoke in aircraft and laboratory studies, *Atmos. Chem. Phys.*, *11*, 12,049–12,064, doi:10.5194/acp-11-12049-2011.

Cusack, M., A. Alastuey, N. Pérez, J. Pey, and X. Querol (2012), Trends of particulate matter ($PM_{2.5}$) and chemical composition at a regional background site in the Western Mediterranean over the last nine years (2002–2010), *Atmos. Chem. Phys.*, *12*, 8341–8357.

De Gouw, J., and C. Warneke (2007), Measurements of volatile organic compounds in the Earth's atmosphere using proton-transfer-reaction mass spectrometry, *Mass Spectrom. Rev.*, *26*(2), 223–257.

DeCarlo, P. F., et al. (2006), Field-deployable, high-resolution, time-of-flight aerosol mass spectrometer, *Anal. Chem.*, *78*, 8281–8289.

DeCarlo, P. F., et al. (2010), Investigation of the sources and processing of organic aerosol over the Central Mexican Plateau from aircraft measurements during MILAGRO, *Atmos. Chem. Phys.*, *10*, 5257–5280, doi:10.5194/acp-10-5257-2010.

Draxler, R. R., and G. D. Rolph (2003), HYSPLIT (HYbrid Single-Particle Lagrangian Integrated Trajectory) Model access via NOAA ARL READY Website (http://www.arl.noaa.gov/ready/hysplit4.html), NOAA Air Resources Laboratory, Silver Spring, Md.

Escudero, M., S. Castillo, X. Querol, A. Ávila, M. Alarcón, M. M. Viana, A. Alastuey, E. Cuevas, and S. Rodriguez (2005), Wet and dry African dust episodes over eastern Spain, *J. Geophys. Res.*, *110*, D18S08, doi:10.1029/2004JD004731.

Filella, I., and J. Peñuelas (2006), Daily, weekly and seasonal time courses of VOCs concentrations in a semi-urban area near Barcelona, *Atmos. Environ.*, *40*, 7752–7769.

used in this publication. The authors wish to thank the Catalan Meteorological Service for providing the BCN radio-sounding data. Finally, we would like to express our gratitude to Jesús Parga for his technical support.

Gangoiti, G., M. M. Millán, R. Salvador, and E. Mantilla (2001), Long range transport and re-circulation of pollutants in the Western Mediterranean during the RECAPMA Project, *Atmos. Environ.*, *35*, 6267–6276.

Graus, M., M. Müller, and A. Hansel (2010), High resolution PTR-TOF: Quantification and formula confirmation of VOC in real time, *J. Am. Soc. Mass Spectrom.*, *21*, 1037–1044.

Heald, C. L., et al. (2010), A simplified description of the evolution of organic aerosol composition in the atmosphere, *Geophys. Res. Lett.*, *37*, L08803, doi:10.1029/2010GL042737.

Hellen, H., P. Kuronen, and H. Hakola (2012), Heated stainless steel tube for ozone removal in the ambient air measurements of mono- and sesquiterpenes, *Atmos. Environ.*, *57*, 35–40.

Holben, B. N., et al. (1998), AERONET—A federated instrument network and data archive for aerosol characterization, *Remote Sens. Environ.*, *66*(1), 1–16.

Holzworth, C. G. (1964), Estimates of mean maximum mixing depths in the contiguous United States, *Mon. Weather Rev.*, *92*, 235–242.

Ichoku, C., D. A. Chu, S. Mattoo, Y. J. Kaufman, L. A. Remer, D. Tanre, I. Slutsker, and B. N. Holben (2002), A spatio-temporal approach for global validation and analysis of MODIS aerosol products, *Geophys. Res. Lett.*, *29*(12), 8006, doi:10.1029/2001GL013206.

Jimenez, J. L., et al. (2009), Evolution of organic aerosols in the atmosphere, *Science*, *326*, 1525–1529.

Jorba, O., et al. (2013), Meteorological overview and transport patterns of the DAURE field campaign: Link to PM observations, *Atmos. Environ.*, *77*, 607–620.

Karanasiou, A., K. Eleftheriadis, S. Vratolis, P. Zarbas, N. Mihalopoulos, C. Mitsakou, C. Housiadas, M. Lazaridis, J. Ondracek, and L. Dzumbova (2008), Size distribution of inorganic species and their inhaled dose in a detergent industrial workplace, *Water Air Soil Pollut. Focus*, *8*, 71–76, doi:10.1007/s11267-007-9140-z.

Knote, C., et al. (2011), Towards an online-coupled chemistry-climate model: Evaluation of trace gases and aerosols in COSMO-ART, *Geosci. Model Dev.*, *4*, 1077–1102, doi:10.5194/gmd-4-1077-2011.

Lanz, V. A., et al. (2010), Characterization of aerosol chemical composition with aerosol mass spectrometry in Central Europe: An overview, *Atmos. Chem. Phys.*, *10*, 10,453–10,471.

Lelieveld, J., et al. (2002), Global air pollution crossroads over the Mediterranean, *Science*, *298*, 794–799.

Lindinger, W., A. Hansel, and A. Jordan (1998), On-line monitoring of volatile organic compounds at pptv levels by means of proton-transfer-reaction mass spectrometry (PTR-MS)—Medical applications, food control and environmental research, *Int. J. Mass Spectrom.*, *173*, 191–241.

Llusia, J., J. Peñuelas, R. Seco, and I. Filella (2012), Seasonal changes in the daily emission rates of terpenes by Quercus ilex and the atmospheric concentrations of terpenes in the natural park of Montseny, NE Spain, *J. Atmos. Chem.*, *69*, 215–230, doi:10.1007/s10874-012-9238-1.

Lopez-Bustins, J. A., J. Martin-Vide, and A. Sanchez-Lorenzo (2008), Iberian winter rainfall trends based upon changes in teleconnection and circulation patterns, *Global Planet. Change*, *63*, 171–176.

Millán, M. M., B. Artíñano, L. A. Alonso, M. Navazo, and M. Castro (1991), The effect of meso-scale flows on the regional and long-range atmospheric transport in the western Mediterranean area, *Atmos. Environ.*, *25A*, 949–963.

Millán, M. M., R. Salvador, E. Mantilla, and G. Kallos (1997), Photooxidant dynamics in the Mediterranean basin in summer: Results from European research projects, *J. Geophys. Res.*, *102*, 8811–8823, doi:10.1029/96JD03610.

Minguillón, M. C., et al. (2011), Fossil versus contemporary sources of fine elemental and organic carbonaceous particulate matter during the DAURE campaign in Northeast Spain, *Atmos. Chem. Phys.*, *11*, 12,067–12,084.

Mohr, C., et al. (2012), Identification and quantification of organic aerosol from cooking and other sources in Barcelona using aerosol mass spectrometer data, *Atmos. Chem. Phys.*, *12*, 1649–1665.

Moreno, T., et al. (2011), Variations in time and space of trace metal aerosol concentrations in urban areas and their surroundings, *Atmos. Chem. Phys.*, *11*, 9415–9430.

Ng, N. L., M. R. Canagaratna, J. L. Jimenez, Q. Zhang, I. M. Ulbrich, and D. R. Worsnop (2011), Real-time methods for estimating organic component mass concentrations from aerosol mass spectrometer data, *Environ. Sci. Technol.*, *45*, 910–916.

Pappalardo, G., et al. (2007), EARLINET-ASOS: European Aerosol Research Lidar Network-Advanced Sustainable Observation System, paper presented at Annual Meeting, Am. Meteor. Soc., San Antonio, Tex.

Pérez, C., M. Sicard, O. Jorba, A. Comeron, and J. M. Baldasano (2004), Summertime re-recirculations of air pollutants over the North-Eastern Iberian coast observed from systematic EARLINET Lidar measurements in Barcelona, *Atmos. Environ.*, *38*, 3983–4000.

Pérez, N., J. Pey, S. Castillo, M. Viana, A. Alastuey, and X. Querol (2008a), Interpretation of the variability of levels of regional background aerosols in the Western Mediterranean, *Sci. Total Environ.*, *407*, 527–540.

Pérez, N., J. Pey, X. Querol, A. Alastuey, J. M. Lopez, and M. Viana (2008b), Partitioning of major and trace components in PM_{10}–$PM_{2.5}$–PM_1 at an urban site in Southern Europe, *Atmos. Environ.*, *42*, 1677–1691.

Pérez, N., J. Pey, M. Cusack, C. Reche, X. Querol, A. Alastuey, and M. Viana (2010), Variability of particle number, black carbon, and PM10, PM2.5 and PM1 levels and speciation: Influence of road traffic emissions on urban air quality, *Aerosol Sci. Technol.*, *44*, 487–499.

Pey, J., S. Rodríguez, X. Querol, A. Alastuey, T. Moreno, J. P. Putaud, and R. Van Dingenen (2008), Variations of urban aerosols in the western Mediterranean, *Atmos. Environ.*, *42*, 9052–9062.

Pey, J., N. Pérez, S. Castillo, M. Viana, T. Moreno, M. Pandolfi, J. M. Lopez-Sebastian, A. Alastuey, and X. Querol (2009), Geochemistry of regional background aerosols in the Western Mediterranean, *Atmos. Res.*, *94*, 422–435.

Pey, J., N. Pérez, X. Querol, A. Alastuey, M. Cusack, and C. Reche (2010), Intense winter atmospheric pollution episodes affecting the Western Mediterranean, *Sci. Total Environ.*, *408*, 1951–1959.

Pey, J., X. Querol, A. Alastuey, F. Forastiere, and M. Stafoggia (2013), African dust outbreaks over the Mediterranean Basin during 2001–2011: PM10 concentrations, phenomenology and trends, and its relation with synoptic and mesoscale meteorology, *Atmos. Chem. Phys.*, *13*, 1395–1410, doi:10.5194/acp-13-1395-2013.

Querol, X., A. Alastuey, J. A. Puicercus, E. Mantilla, J. V. Miró, A. Lopez-Soler, F. Plana, and B. Artinano (1998), Seasonal evolution of suspended particles around a large coal-fired power station: Particles levels and sources, *Atmos. Environ.*, *32*(11), 1963–1978.

Querol, X., A. Alastuey, S. Rodríguez, F. Plana, E. Mantilla, and C. R. Ruiz (2001), Monitoring of PM10 and PM2.5 around primary particulate anthropogenic emission sources, *Atmos. Environ.*, *35*, 845–858.

Querol, X., A. Alastuey, J. Pey, M. Cusack, N. Pérez, N. Mihalopoulos, C. Theodosi, E. Gerasopoulos, N. Kubilay, and M. Koçak (2009), Variability in regional background aerosols within the Mediterranean, *Atmos. Chem. Phys.*, *9*, 4575–4591, doi:10.5194/acp-9-4575-2009.

Querol, X., et al. (2004), Levels of PM in rural, urban and industrial sites in Spain, *Sci. Total Environ.*, *334–335*, 359–376.

Querol, X., et al. (2008a), PM speciation and sources in Mexico during the MILAGRO-2006 Campaign, *Atmos. Chem. Phys.*, *8*, 111–128.

Querol, X., et al. (2008b), Spatial and temporal variations in airborne particulate matter (PM_{10} and $PM_{2.5}$) across Spain 1999–2005, *Atmos. Environ.*, *42*(17), 3964–3979.

Querol, X., et al. (2013), Variability of carbonaceous aerosols in remote, rural, urban and industrial environments in Spain: Implications for air quality policy, *Atmos. Chem. Phys.*, *13*, 6185–6206, doi:10.5194/acp-13-6185-2013.

Reche, C., et al. (2011a), Peculiarities in atmospheric particle number and size-resolved speciation in an urban area in the western Mediterranean: Results from the DAURE campaign, *Atmos. Environ.*, *45*(30), 5282–5293.

Reche, C., et al. (2011b), New considerations for PM, black carbon and particle number concentration for air quality monitoring across different European cities, *Atmos. Chem. Phys.*, *11*, 6207–6227.

Reche, C., et al. (2012), Biomass burning contributions to urban aerosols in a coastal Mediterranean City, *Sci. Total Environ.*, *427–428*, 175–190.

Rocadenbosch, F., C. Soriano, A. Comerón, J. M. Baldasano, A. Rodríguez, C. Muñoz, and D. García-Vizcaíno (2000), 3D scanning portable backscatter lidar platform for atmospheric remote sensing: Performance and architecture overview, *Proc. SPIE Int. Soc. Opt. Eng.*, *4168*, 158–169.

Rodríguez, S., X. Querol, A. Alastuey, G. Kallos, and O. Kakaliagou (2001), Saharan dust contributions to PM_{10} and TSP levels in Southern and Eastern Spain, *Atmos. Environ.*, *35*, 2433–2447.

Rodríguez, S., X. Querol, A. Alastuey, M. M. Viana, and E. Mantilla (2003), Events affecting levels and seasonal evolution of airborne particulate matter concentrations in the Western Mediterranean, *Environ. Sci. Technol.*, *37*, 216–222.

Schnitzhofer, R., J. Beauchampa, J. Dunkl, A. Wisthaler, A. Weber, and A. Hansel (2008), Long-term measurements of CO, NO, NO_2, benzene, toluene and PM_{10} at a motorway location in an Austrian valley, *Atmos. Environ.*, doi:10.1016/j.atmosenv.2007.10.004.

Schnitzhofer, R., A. Wisthaler, and A. Hansel (2009), Real-time profiling of organic trace gases in the planetary boundary layer by PTR-MS using a tethered balloon, *Atmos. Meas. Tech.*, *2*, 773–777, doi:10.5194/amt-2-773-2009.

Seco, R., J. Peñuelas, and I. Filella (2007), Short-chain oxygenated VOCs: Emission and uptake by plants and atmospheric sources, sinks, and concentrations, *Atmos. Environ.*, *41*, 2477–2499, doi:10.1016/j.atmosenv.2006.11.029.

Seco, R., J. Peñuelas, I. Filella, J. Llusià, R. Molowny-Horas, S. Schallhart, A. Metzger, M. Müller, and A. Hansel (2011), Contrasting winter and summer VOC mixing ratios at a forest site in the Western Mediterranean Basin: The effect of local biogenic emissions, *Atmos. Chem. Phys.*, *11*, 13,161–13,179, doi:10.5194/acp-11-13161-2011.

Seco, R., J. Peñuelas, I. Filella, J. Llusia, S. Schallhart, A. Metzger, M. Müller, and A. Hansel (2013), Volatile organic compounds in the western Mediterranean basin: Urban and rural winter measurements during the DAURE campaign, *Atmos. Chem. Phys.*, *13*, 4291–4306, doi:10.5194/acp-13-4291-2013.

Sicard, M., F. Rocadenbosch, M. N. M. Reba, A. Comerón, S. Tomás, D. García-Vízcaino, O. Batet, R. Barrios, D. Kumar, and J. M. Baldasano (2011), Seasonal variability of aerosol optical properties observed by means of a Raman Lidar at an EARLINET site over Northeastern Spain, *Atmos. Chem. Phys.*, *11*, 175–190, doi:10.5194/acp-11-175-2011.

Stohl, A., C. Forster, S. Eckhardt, N. Spichtinger, H. Huntrieser, J. Heland, H. Schlager, S. Wilhelm, F. Arnold, and O. Cooper (2003), A backward modeling study of intercontinental pollution transport using aircraft measurements, *J. Geophys. Res.*, *108*(D12), 4370, doi:10.1029/2002JD002862.

Stohl, A., C. Forster, A. Frank, P. Seibert, and G. Wotawa (2005), Technical note: The Lagrangian particle dispersion model FLEXPART version 6.2, *Atmos. Chem. Phys.*, *5*, 2461–2474.

Szidat, S. (2009), Sources of Asian haze, *Science*, *323*, 470–471.

Szidat, S., A. S. H. Prevot, J. Sandradewi, M. R. Alfarra, H.-A. Synal, L. Wacker, and U. Baltensperger (2007), Dominant impact of residential wood burning on particulate matter in Alpine valleys during winter, *Geophys. Res. Lett.*, *34*, L05820, doi:10.1029/2006GL028325.

Takegawa, N., Y. Miyazaki, Y. Kondo, Y. Komazaki, T. Miyakawa, J. L. Jimenez, J. T. Jayne, D. R. Worsnop, J. D. Allan, and R. J. Weber (2005), Characterization of an aerodyne aerosol mass spectrometer (AMS): Intercomparison with other aerosol instruments, *Aerosol Sci. Technol.*, *39*(8), 760–770.

Thorpe, A., and R. M. Harrison (2008), Sources and properties of non-exhaust particulate matter from road traffic: A review, *Sci. Total Environ.*, *400*(1–3), 270–282, doi:10.1016/j.scitotenv.2008.06.007.

van Drooge, B. L., M. Crusack, C. Reche, C. Mohr, A. Alastuey, X. Querol, A. S. H. Prevot, D. A. Day, J. L. Jimenez, and J. O. Grimalt (2012), Molecular marker characterization of the organic composition of submicron aerosols from Mediterranean urban and rural environments under contrasting meteorological conditions, *Atmos. Environ.*, *61*, 482–489.

Viana, M., C. Pérez, X. Querol, A. Alastuey, S. Nickovic, and J. M. Baldasano (2005), Spatial and temporal variability of PM levels and composition in a complex summer atmospheric scenario in Barcelona (NE Spain), *Atmos. Environ.*, *39*, 5343–5361.

White, M. L., et al. (2009), Are biogenic emissions a significant source of summertime atmospheric toluene in the rural Northeastern United States?, *Atmos. Chem. Phys.*, *9*, 81–92, doi:10.5194/acp-9-81-2009.

Zhang, Q., D. R. Worsnop, M. R. Canagaratna, and J. L. Jimenez (2005), Hydrocarbon-like and oxygenated organic aerosols in Pittsburgh: Insights into sources and processes of organic aerosols, *Atmos. Chem. Phys.*, *5*, 3289–3311.

Zhang, Q., et al. (2007), Ubiquity and dominance of oxygenated species in organic aerosols in anthropogenically-influenced Northern Hemisphere midlatitudes, *Geophys. Res. Lett.*, *34*, L13801, doi:10.1029/2007GL029979.

Zhang, Y. L., N. Perron, V. G. Ciobanu, P. Zotter, M. C. Minguillon, L. Wacker, A. S. H. Prevot, U. Baltensperger, and S. Szidat (2012), On the isolation of OC and EC and the optimal strategy of radiocarbon-based source apportionment of carbonaceous aerosols, *Atmos. Chem. Phys.*, *12*, 10,841–10,856.

Zheng, G., Y. Cheng, K. He, F. Duan, and Y. Ma (2014), A newly identified calculation discrepancy of the Sunset semi-continuous carbon analyzer, *Atmos. Meas. Tech. Discuss.*, *7*, 377–399, doi:10.5194/amtd-7-377-2014.